Fig. 2. TEM analysis of skin, lymph node, liver and brain samples from mice after 28-days of dermal exposure to silica nanoparticles and quantum dots. a–c, nSP70 (arrows) were present in the nucleus of skin (a), cervical lymph node (b), and parenchymal hepatocytes (c). d, nSP70 were also detected in the mitochondria of parenchymal hepatocytes. e–f, nSP70 were found in neuron of the cerebral cortex (e) and the hippocampus (f). g–h, QD (arrows) were present in the nucleus of skin (g), cervical lymph node (h) and parenchymal hepatocytes (i), similar to nSP70. j, In parenchymal hepatocytes, QD were detected in the mitochondria (j). k–l, QD were found in neuron of the cerebral cortex (k) and the hippocampus (l). N: nucleus; M: mitochondria. Scale bars: 200 nm (a, e–g, and j–l), 500 nm (b–d, h and i).
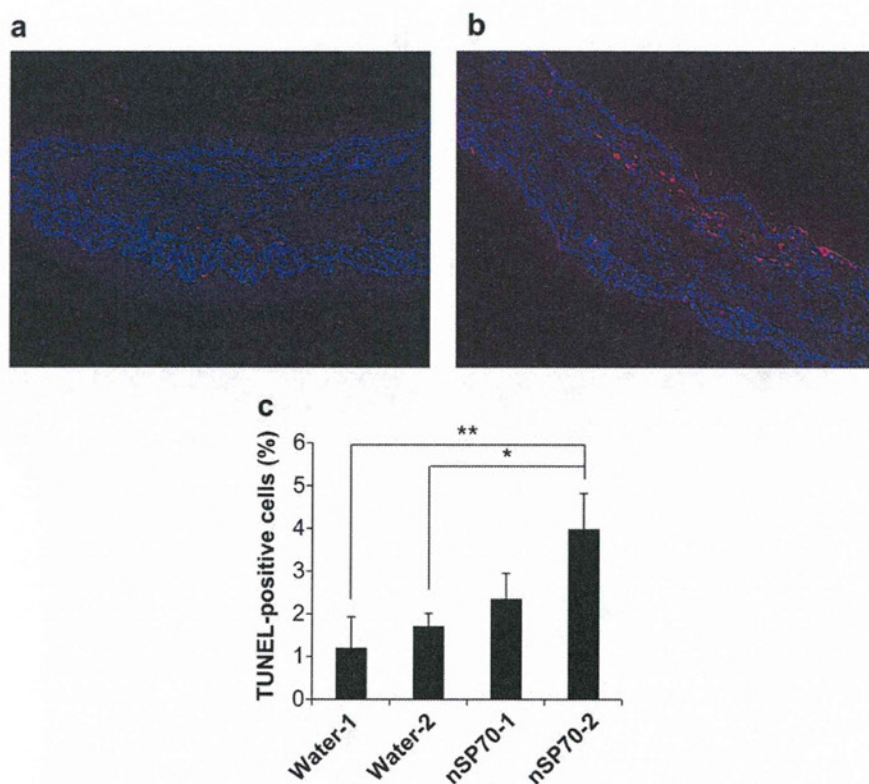
Fig. 3. Detection of apoptotic cells in silica nanoparticles-applied mice skin. a, b, Representative images from TUNEL stained skin section in water- (control, a) and nSP70- (b) applied mice were shown. Nuclei and TUNEL-positive cells were represented in blue and red, respectively. Original magnification, ×200. c, For quantification of TUNEL-positive cells, approximately 1000 cells were randomly selected from 3 different areas in each section and two animals and counted the numbers of positive cells expressed as a percentage of the total (c). Data shown are average means (±SD) of each treated group. * Significant increase ($P < 0.005$) compared with Water-2. ** Significant increase ($P < 0.001$) compared with Water-1.

distributions and biological responses of NM size in skin with a focus on nSP.

3.4. Analysis of intracellular distribution of silica particles in human keratinocyte

Presently, many modern cosmetic or sunscreen products contain nano-sized components, such as titanium dioxide (TiO_2), zinc oxide (ZnO) and amorphous silica particles. Nano-sized TiO_2 and ZnO are colorless substances and reflect/scatter ultraviolet (UV) more efficiently than their larger counterparts [28,29]. Amorphous nanosilica particles (nSPs) are used in large quantities and are one of the most important ingredients in the cosmetic industry, especially for their light-diffusing and absorption properties. Extensive consumption of these NM-supplemented cosmetic and food products has naturally raised the question as to whether these NMs could penetrate the skin, would eventually become absorbed systemically, and more importantly, whether they could be responsible for acute/chronic side effects. In the present study, we revealed that well-dispersed nSP could penetrate into and pass through the skin. Interestingly, we found that nSP70 migrated into the blood stream and passed into tissues such as liver. Moreover, nSP70 invaded specific organelles such as the nucleus and mitochondria. In view of these observations, we next examined the relation between the intracellular distribution and biological effects of nSP, which are the most important NMs in our daily life.

To determine the intercellular location of silica particles, we used TEM to examine the HaCaT cells that were treated with 100 µg/ml of nSP70, nSP300, or mSP1000. TEM examination revealed the presence of mSP1000 and nSP300 only in the endosome (Fig. 4a, b, arrows). mSP1000-treated cells were also found to contain a large number of lysosomes (Fig. 4a). In contrast, only in the nSP70-treated cells nSP70s were present in the cytoplasm as well as in the nucleus (Fig. 4c, d, arrow heads). Furthermore, nSP70s were accumulated in the nucleolus (Fig. 4e, f, arrows). Recently, it has been reported that the intercellular localization of NM is possibly linked to the induction of harmful effects. For example, the localization of silver nanoparticles in the nucleus and mitochondria may be related to mitochondrial dysfunction or oxidative stress [30]. Thus, analysis of intracellular localization enables us to provide important and useful information to predict the hazard to human health.

3.5. Analysis of cell-growth inhibition and genotoxicity induced by silica particles

Next, we investigated the biological effects of nSP. To this end, we assessed the effects of various particle size nSP on the proliferation of HaCaT cells. As shown in Fig. 5a, cell proliferation was inhibited following treatment with nSP70 and nSP300 in both dose and size dependent manner. The half maximal (50%) inhibitory concentration (IC_{50}) of nSP70 and nSP300 for inhibiting cell proliferation was 323 and 3966 µg/ml, respectively. We were, however, unable to calculate the IC_{50} of nSP1000. Taken together, these results suggested that smaller sized silica particles inhibited the growth of HaCaT cells more strongly than the larger particles. In addition, we assessed the effects of QD on the proliferation of HaCaT cells. As the result, we indicated that the effect to cell proliferation of QD was predominantly lower than nSP70 at same
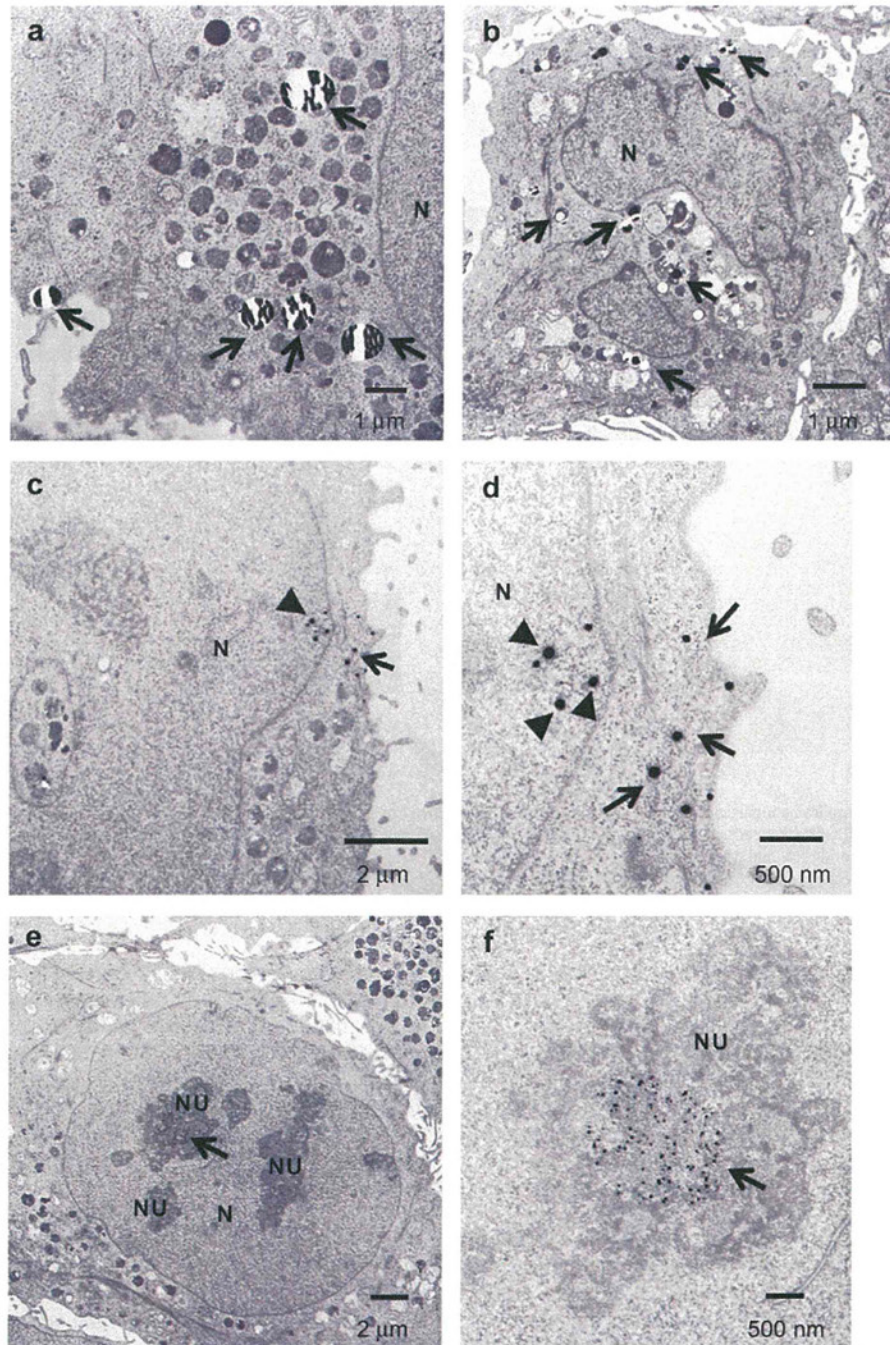
Fig. 4. TEM analysis of HaCaT cells treated with silica particles. a–e, Silica particles (arrows) were found in HaCaT cells treated for 24 h with 100 μg/ml of mSP1000 (a), nSP300 (b), and nSP70 (c, d, and e). In panels c and d, arrow heads show the presence of nSP70 in the nucleus, and in panels e and f, arrows show the presence of nSP70 in the nucleolus. Panels d and f are same as panels c and e at higher magnifications, respectively. N: nucleus; NU: nucleolus. Scale bars: 1 μm (a and b), 2 μm (c and e) and 500 nm (d and f).

concentrations (particles/ml) (Fig. 5b). This result suggested that the biological effects of NMs were different by material.

On the basis of the nuclear entry of nSP70 *in vivo* and *in vitro*, we next evaluated the mutagenicity of silica particles using *S. typhimurium* strains TA98 and TA100 (Ames test). None of the nSP that we tested induced mutation in TA98 strain when used at the indicated concentrations (Fig. 6a). By contrast, nSP of all sizes induced mutagenicity in TA100 strain at the highest dose of treatment (810 μg/ml) (Fig. 6b). At lower doses (30 and 90 μg/ml) of

treatment, only nSP70 induced mutation in TA100 strain (Fig. 6b). Thus, the results obtained from the Ames test suggest that the mutagenicity of the silica particles increased with the decreasing particle size. Next, we used the comet assay to analyze DNA single strand breaks in nSP-treated HaCaT cells. In cells treated with PBS (negative control) for 3 h, the average tail length was 23.3 μm (Fig. 6c). In cells treated with 90 μg/ml of nSP70, nSP100, nSP300, or mSP1000, the average tail lengths were 102.9 μm (Fig. 6d), 88.8 μm (data not shown), 30.5 μm (Fig. 6e), and 22.5 μm (Fig. 6f), respectively.
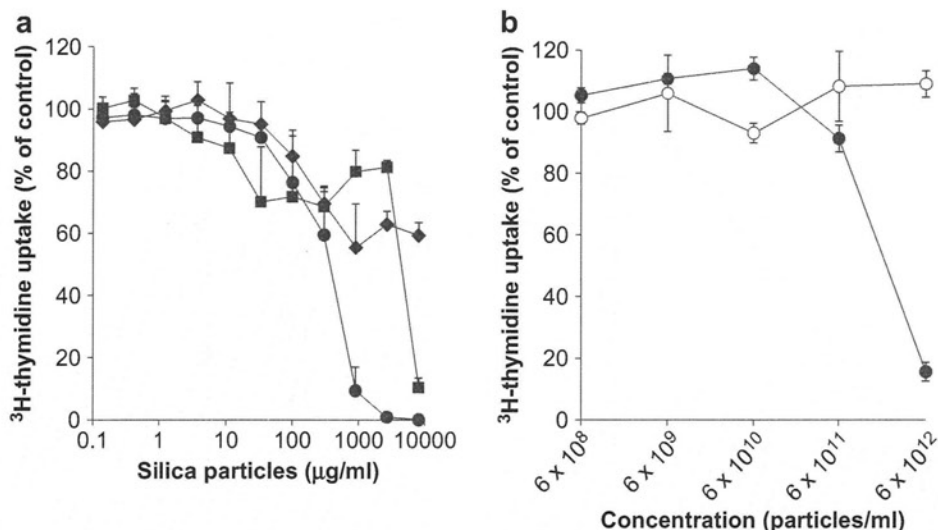
Fig. 5. Effect of various sized silica particles and QDs on cell proliferation. a) In order to assess the biological effects according to particle size, proliferation of HaCaT cells following 24 h of incubation with the indicated concentrations of nSP70 (closed circle), nSP300 (closed square) and mSP1000 (closed diamond) were measured using the tritium thymidine uptake assay. b) In order to assess the biological effects according to the material, proliferation of HaCaT cells following 24 h of incubation with the indicated concentrations of nSP70 (closed circle) and QD (opened circle) were measured. Results shown as relative rates (% of control). Each data point represents mean ± SD ($n = 3$).

The average tail lengths increased depending on the dose and size of the silica particles (Fig. 6g). The tail lengths found in the nSP70- and nSP100-treated cells were longer than those found in the positive control cells (0.2 mM H_2O_2 treated cells). These findings suggest the possibility that nSP with particle sizes below 100 nm could induce mutation.

3.6. Analysis of in vivo biodistribution of silica particles in mice

We next analyzed biodistribution and biological effects in systemic level using silica particles-injected mice, because it was suggested that nSP moved to the blood stream from skin as described above. To elucidate the *in vivo* distribution of silica particles, we determined the distribution of silica particles following intravenous injection, by optical imaging analysis (Fig. 7a–c). Intense fluorescence was observed near the liver in all silica particle-treated mice immediately after treatment and this signal migrated to near the intestinal tract with time. Imaging of dissected liver from nSP300- or mSP1000-treated mice revealed that intense fluorescence was observed only around the gall bladder. In contrast, nSP70-derived fluorescence was observed throughout dissected liver. In addition, our preliminary results revealed that all silica particle-derived fluorescence was also observed in intestinal tract and feces (data not shown), suggesting that silica particles might be excreted in the bile after circulating systemically, in a manner independent of particle size.

To clarify detailed localization of silica particles in liver of nSP-injected mice, next we perform transmission electron microscopy (TEM) analysis (Fig. 7d–g). While silica particles of all sizes were found to be ingested into Kupffer cells, nSP70 and nSP300 were also observed in parenchymal hepatocytes. In the nSP70-treated group, particles were shown to be localized in the cytoplasm and nucleus of various tissues such as lung, kidney, spleen and lymph node (data not shown). Microscopic findings showed that with reduction in particle size, silica particle uptake into Kupffer cells tended to be decreased and in contrast, particle uptake into the cytoplasm of parenchymal hepatocytes tended to be increased (Fig. 7h). Surprisingly, sub-nuclear localization of particles was observed in nSP70-treated groups (Fig. 7e). These results confirmed that the

distribution of nSPs with particle size less than 100 nm differ from those of submicron-sized silica particles. These data strongly suggested that we must distinguish nSPs from existing submicron-sized silica particles, and address specialized risk assessment for nSPs.

3.7. Analysis of cytotoxicity and genotoxicity in primary hepatocyte induced by silica particles

Subsequently, we confirmed whether the biological effects induced by nSP in liver in which silica particles accumulated. The liver is one of the most important tissue in the body, because the liver takes an important role in metabolism, discharge, detoxication, maintenance of homeostasis of the body fluid. Especially, hepatocyte plays a vital role as functions of the liver. Using primary hepatocyte isolated from silica particles-injected mice intravenously, cytotoxicity and DNA damage of hepatocyte were analyzed. As the result, cytotoxicity of hepatocyte from nSP300 and mSP1000-injected mice little occurred. On the other hand, hepatocyte from nSP70-injected mice indicated higher cytotoxicity than nSP300 and mSP1000-injected mice (Fig. 8a). Furthermore, DNA damage of hepatocyte was detected only in nSP70-injected mice as well as in HaCaT cells (Fig. 8b). These results also indicate that differences in biological effects such as cytotoxicity and genotoxicity are caused by differences in biodistribution of silica particles. And it suggests that accumulation of nSP into the liver and/or nucleus may lead to genotoxicity.

Thus, we also highly recommend including carcinogenicity test and reproductive and developmental toxicity test for ensuring biosafety of NMs. Additionally, because nSP70 were accumulated in the nucleus, we suggest evaluating the effect of an NM on protein synthesis to further ensure its biosafety.

Nuclear pores are made of large protein complexes that cross the nuclear envelope, the membrane bilayer that surrounds the nucleus of the eukaryotic cell, and the pores are about 30 nm in diameter [31,32]. Thus, it is unlikely that the nSP70, which has a mean diameter of about 70 nm, entered the nucleus through the nuclear pore. We hypothesize that the nSP70 might interact with the nuclear transporting proteins via specific- or non-specific
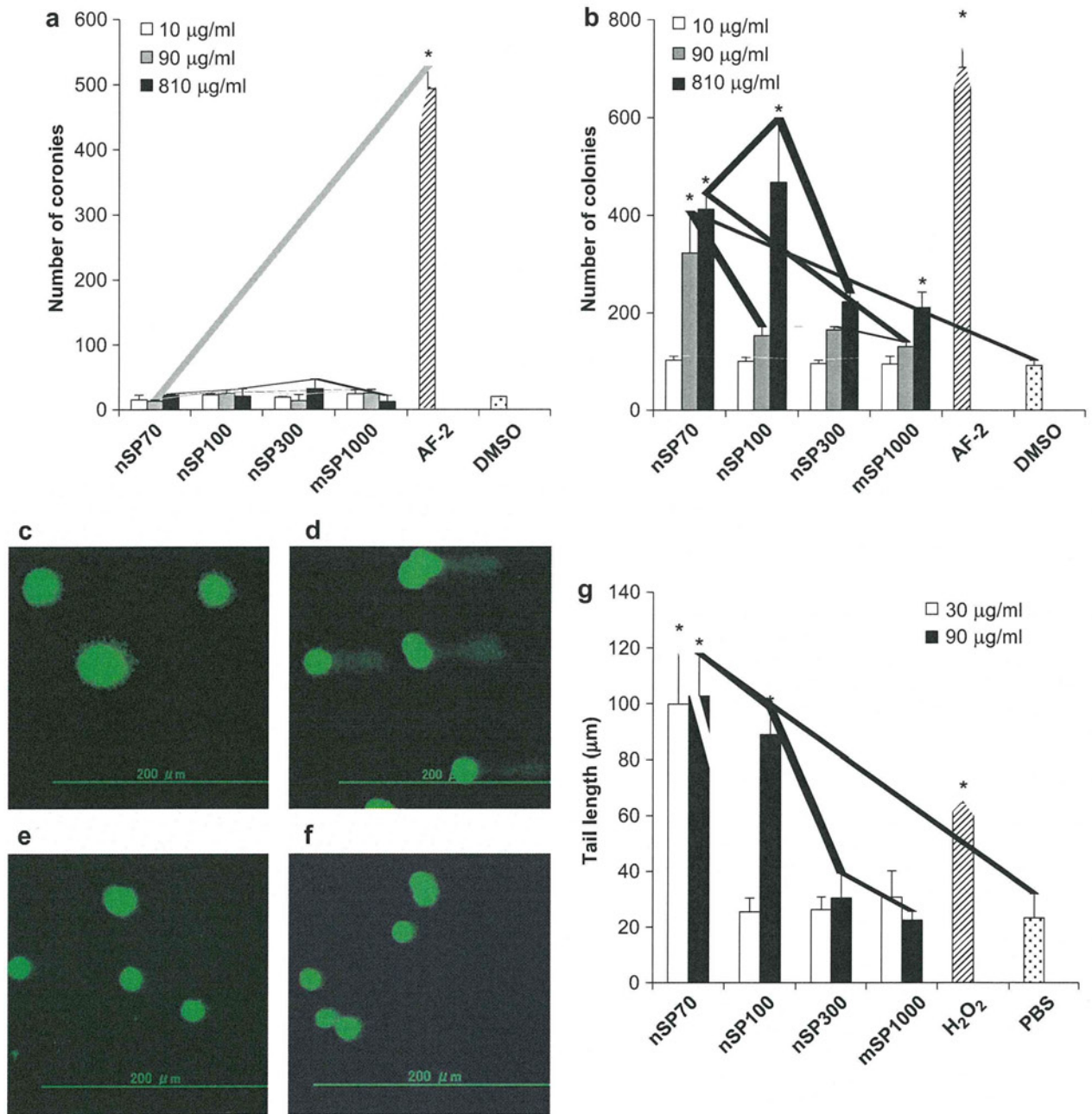
Fig. 6. Genotoxic effects of silica particles. a–b, Mutagenic effects of silica particles as determined by the Ames test. Dose-response of mutagenic effects of nSP70, nSP300, and mSP1000 on *S. typhimurium* strains: strain TA98 (a) and strain TA100 (b). The Ames test was performed as described in Methods. Values shown are mean ± SD ($n = 3$). *More than 2-fold increase compared to the medium-treated control (DMSO). AF-2, positive control. e–g, Detection of DNA strand breaks by the comet assay. Representative fluorescence images of HaCaT cells treated for 3 h with PBS (negative control) (c), or 90 μg/ml of nSP70 (d), nSP300 (e), and mSP1000 (f). Scale bar: 200 μm e, Column graph showing the tail lengths after being incubated with 30 μg/ml (open column) and 90 μg/ml (closed column), respectively, of nSP70, nSP300, and mSP1000, and 0.2 mM H_2O_2 (positive control) for 3 h. Data shown are average means (±SD) of at least 16 cells for each sample. Results shown are representative of more than three independent experiments. *Significant increase ($P < 0.01$) compared with the negative control, PBS.

interactions, and the nSP70/protein complexes are then transported into the nucleus. To test this hypothesis, we are currently pursuing a proteome-based approach to identify nSP70-interacting proteins.

Recently, commercially available amorphous silica-based products were subjected to various toxicological tests including acute and repeated dose toxicity, genotoxicity, carcinogenicity and reproductive toxicity [33]. According to this report, amorphous silica particles are non-toxic. Although the primary particle sizes of the amorphous silica used in these toxicological studies were between 1 and 100 nm, the ECETOC 2006 report stated that they did not exist as primary particles, but existed only as aggregates of particle sizes between 100 nm and 1 μm. The ECETOC 2006 report, however, did not exclude the possibility that materials having particle sizes below 100 nm might be developed and available for use in the future. In contrast to the results described in the ECETOC report, results of our present
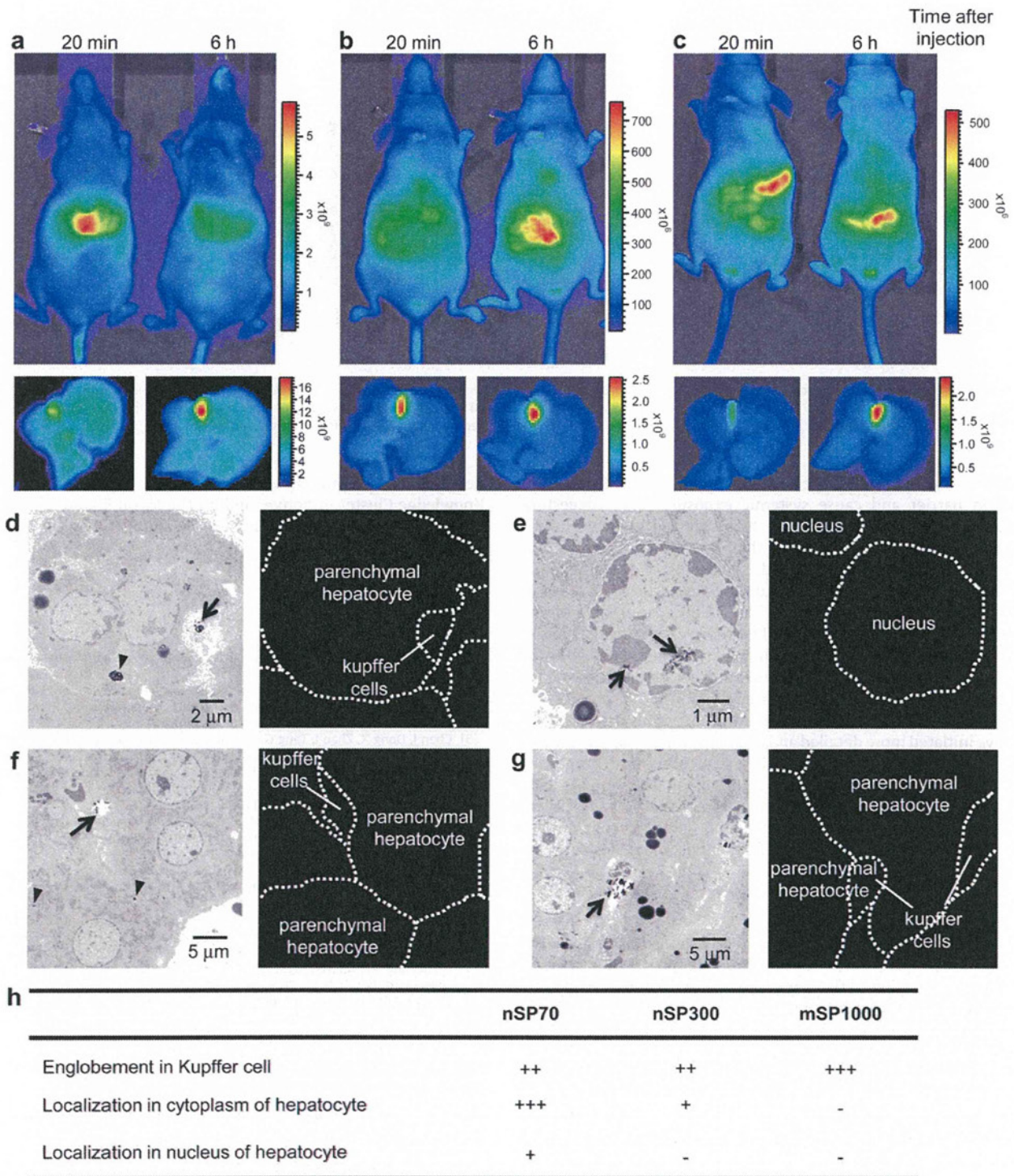
Fig. 7. Biodistribution analysis of silica particles at macro- and micro levels. A–C, Macro level analysis: optical imaging of fluorescently labeled silica particles in live mice and excised liver. DY676-labeled silica particles (a, nSP70, b, nSP300 and c, mSP1000, 100 mg/kg) were intravenously injected into female hairless mice. Twenty min and 6 h after injection, optical images were acquired using a Xenogen IVIS 200 imaging system. The signal intensity in the region of interest is expressed as photons (p) per second (sec) per centimeter squared (cm^2) per steradian (sr) (a steradian is a unit of solid angle). d–f, Micro level analysis: BALB/c mouse liver injected with 30 mg/kg (nSP70) or 100 mg/kg (nSP300 and mSP1000) nSPs was observed by TEM. d, arrow, nSP70, f arrow, nSP300, g, mSP1000 were phagocytosed in Kupffer cells. d, arrow head, nSP70 and f, arrow head, nSP300 were also detected in cytoplasm of parenchymal hepatocytes. Interestingly, e, nSP70 entered the nucleus of the parenchymal hepatocytes. Arrows and arrow heads indicate silica particles. Scale bar, d, 2 μm, e, 1 μm and f, g, 5 μm. H, Localization of each silica particle in liver is summarized. Amount of silica particles were shown as follows; –: Not detected, +: small, ++: middle, +++: large.
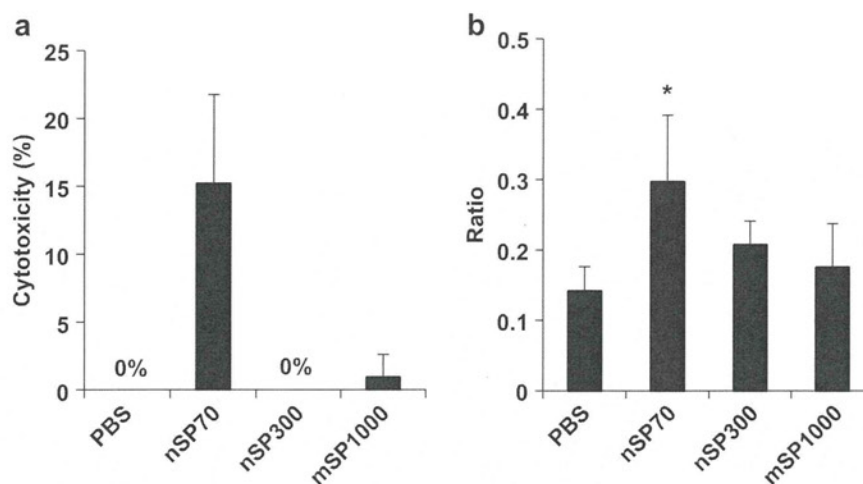
Fig. 8. Liver toxicity analysis in parenchymal hepatocytes. a, Cytotoxicity of parenchymal hepatocytes isolated from nSP-injected mice 5 h after injection by trypan blue stain. b, Detection of DNA strand breaks ratio of parenchymal hepatocytes isolated from nSP-injected mice 5 h after injection. Data are shown as mean ± SD; comet tails from at least 16 cells were counted in each sample. All data are representative of more than three slides. * Represents significant difference from the control group ($P < 0.01$).

study showed that well-dispersed nSP70 could indeed penetrate the skin barrier and cause systemic exposure, thus suggesting that the well-dispersed NMs have to be viewed as new entities and tested accordingly for ensuring their biosafety. It is known that the asbestos-related health hazard, symptoms of mesothelioma, appears after prolonged exposure to asbestos particles (average of 40 years, shortest around 20 years) [34–37]. Because of this and also in view of the growing demand for the NMs in various fields, there is a clear and urgent need for in depth risk assessment of all NMs for safety use. Keeping in line with this idea and because it is not known whether exposure to NMs might cause initiation and/or progression of various diseases (e.g., atopic dermatitis, infectious disease, etc.), we have initiated more detailed and extensive safety analysis studies including relationships between the physicochemical properties (i.e., size, shape, and surface property) of an NM and its bio-distribution, and analysis of the interaction of the NMs with aller-gens, gastrointestinal flora, and resident floras as contributing factors to human health in order to further ensure its biosafety.

4. Conclusions

This study revealed that, as compared with the bulk material of particle sizes above nanoscale (above 100 nm), well-dispersed amorphous nanosilica with a particle size of 70 nm shows different bio-properties with respect to skin penetration and nuclear entry. These bio-properties of nanosilica show the potential as a new functional material, but, reflecting these differences, nSP70 exert various adverse biological effects in regional and systemic level, such as DNA fragmentation. We consider that more information which provided by further studies of relation between physico-chemical properties and biological responses, would lead to reali-zation of an affluent society by the use of safe and useful NMs.

Acknowledgments

References

[1] Salata O. Applications of nanoparticles in biology and medicine. J Nanobio-technology 2004;2(1):3.
[2] Aiso S, Yamazaki K, Umeda Y, Asakura M, Takaya M, Toya T, et al. Pulmonary toxicity of intratracheally instilled multiwall carbon nanotubes in male Fischer 344 rats. Ind Health; 2010 [Epub ahead of print].
[3] Chen J, Dong X, Zhao J, Tang G. In vivo acute toxicity of titanium dioxide nano-particles to mice after intraperitoneal injection. J Appl Toxicol 2009;29(4):330–7.
[4] Geys J, Nemmar A, Verbeken E, Smolders E, Ratoi M, Hoylaerts MF, et al. Acute toxicity and prothrombotic effects of quantum dots: impact of surface charge. Environ Health Perspect 2008;116(12):1607–13.
[5] Heng BC, Zhao X, Xiong S, Ng KW, Boey FY, Loo JS. Toxicity of zinc oxide (ZnO) nanoparticles on human bronchial epithelial cells (BEAS-2B) is accentuated by oxidative stress. Food Chem Toxicol 2010;48(6):1762–6.
[6] Kocbek P, Teskac K, Kreft ME, Kristl J. Toxicological aspects of long-term treatment of keratinocytes with ZnO and TiO(2) nanoparticles. Small 2010; 6(17):1908–17.
[7] Liu S, Xu L, Zhang T, Ren G, Yang Z. Oxidative stress and apoptosis induced by nanosized titanium dioxide in PC12 cells. Toxicology 2010;267(1–3):172–7.
[8] Moos PJ, Chung K, Woessner D, Honeggar M, Cutler NS, Veranth JM. ZnO particulate matter requires cell contact for toxicity in human colon cancer cells. Chem Res Toxicol 2010;23(4):733–9.
[9] Murray AR, Kisin E, Leonard SS, Young SH, Kommineni C, Kagan VE, et al. Oxidative stress and inflammatory response in dermal toxicity of single-walled carbon nanotubes. Toxicology 2009;257(3):161–71.
[10] Park EJ, Kim H, Kim Y, Yi J, Choi K, Park K. Carbon fullerenes (C60s) can induce inflammatory responses in the lung of mice. Toxicol Appl Pharmacol 2010; 244(2):226–33.
[11] Poland CA, Duffin R, Kinloch I, Maynard A, Wallace WA, Seaton A, et al. Carbon nanotubes introduced into the abdominal cavity of mice show asbestos-like pathogenicity in a pilot study. Nat Nanotechnol 2008;3(7):423–8.
[12] Shin JA, Lee EJ, Seo SM, Kim HS, Kang JL, Park EM. Nanosized titanium dioxide enhanced inflammatory responses in the septic brain of mouse. Neuroscience 2010;165(2):445–54.
[13] Takagi A, Hirose A, Nishimura T, Fukumori N, Ogata A, Ohashi N, et al. Induction of mesothelioma in p53+/− mouse by intraperitoneal application of multi-wall carbon nanotube. J Toxicol Sci 2008;33(1):105–16.
[14] Yamashita K, Yoshioka Y, Higashisaka K, Morishita Y, Yoshida T, Fujimura M, et al. Carbon nanotubes elicit DNA damage and inflammatory response rela-tive to their size and shape. Inflammation 2010;33(4):276–80.
[15] Nabeshi H, Yoshikawa T, Matsuyama K, Nakazato Y, Arimori A, Isobe M, et al. Size-dependent cytotoxic effects of amorphous silica nanoparticles on Lang-erhans cells. Pharmazie 2010;65(3):199–201.
[16] Singh S, Shi T, Duffin R, Albrecht C, van Berlo D, Hohr D, et al. Endocytosis, oxidative stress and IL-8 expression in human lung epithelial cells upon

treatment with fine and ultrafine TiO$_2$: role of the specific surface area and of surface methylation of the particles. Toxicol Appl Pharmacol 2007;222 (2):141–51.

[17] Thibodeau M, Giardina C, Hubbard AK. Silica-induced caspase activation in mouse alveolar macrophages is dependent upon mitochondrial integrity and aspartic proteolysis. Toxicol Sci 2003;76(1):91–101.

[18] Chlopek J, Czajkowaska B, Szaraniec B, Frackowiak E, Szostak K, Beguin F. *In vitro* studies of carbon nanotubes biocompatibility. Carbon 2006;44:1106–11.

[19] Bharali DJ, Klejbor I, Stachowiak EK, Dutta P, Roy I, Kaur N, et al. Organically modified silica nanoparticles: a nonviral vector for *in vivo* gene delivery and expression in the brain. Proc Natl Acad Sci U S A 2005;102(32):11539–44.

[20] Bottini M, D'Annibale F, Magrini A, Cerignoli F, Arimura Y, Dawson MI, et al. Quantum dot-doped silica nanoparticles as probes for targeting of T-lymphocytes. Int J Nanomedicine 2007;2(2):227–33.

[21] Hirsch LR, Stafford RJ, Bankson JA, Sershen SR, Rivera B, Price RE, et al. Nanoshell-mediated near-infrared thermal therapy of tumors under magnetic resonance guidance. Proc Natl Acad Sci U S A 2003;100(23):13549–54.

[22] Roy I, Ohulchanskyy TY, Bharali DJ, Pudavar HE, Mistretta RA, Kaur N, et al. Optical tracking of organically modified silica nanoparticles as DNA carriers: a nonviral, nanomedicine approach for gene delivery. Proc Natl Acad Sci U S A 2005;102(2):279–84.

[23] Verraedt E, Pendela M, Adams E, Hoogmartens J, Martens JA. Controlled release of chlorhexidine from amorphous microporous silica. J Control Release 2010;142(1):47–52.

[24] Ames BN, Gurney EG, Miller JA, Bartsch H. Carcinogens as frameshift mutagens: metabolites and derivatives of 2-acetylaminofluorene and other aromatic amine carcinogens. Proc Natl Acad Sci U S A 1972;69(11):3128–32.

[25] Ames BN, Durston WE, Yamasaki E, Lee FD. Carcinogens are mutagens: a simple test system combining liver homogenates for activation and bacteria for detection. Proc Natl Acad Sci U S A 1973;70(8):2281–5.

[26] McCann J, Spingarn NE, Kobori J, Ames BN. Detection of carcinogens as mutagens: bacterial tester strains with R factor plasmids. Proc Natl Acad Sci U S A 1975;72(3):979–83.

[27] Mortensen LJ, Oberdorster G, Pentland AP, Delouise LA. *In vivo* skin penetration of quantum dot nanoparticles in the murine model: the effect of UVR. Nano Lett 2008;8(9):2779–87.

[28] Nohynek GJ, Lademann J, Ribaud C, Roberts MS. Grey goo on the skin? Nanotechnology, cosmetic and sunscreen safety. Crit Rev Toxicol 2007;37(3): 251–77.

[29] Wolf R, Matz H, Orion E, Lipozencic J. Sunscreens—the ultimate cosmetic. Acta Dermatovenerol Croat 2003;11(3):158–62.

[30] AshaRani PV, Low Kah Mun G, Hande MP, Valiyaveettil S. Cytotoxicity and genotoxicity of silver nanoparticles in human cells. ACS Nano 2009;3(2): 279–90.

[31] Akey CW. Interactions and structure of the nuclear pore complex revealed by cryo-electron microscopy. J Cell Biol 1989;109(3):955–70.

[32] Reichelt R, Holzenburg A, Buhle Jr EL, Jarnik M, Engel A, Aebi U. Correlation between structure and mass distribution of the nuclear pore complex and of distinct pore complex components. J Cell Biol 1990;110(4):883–94.

[33] European Centre for Ecotoxicology and Toxicology of Chemicals (ECETOC). Synthetic Amorphous Silica (CAS No. 7631-86-9). ECETOC JACC Report No.51; 2006.

[34] Enterline PE, Henderson V. Type of asbestos and respiratory cancer in the asbestos industry. Arch Environ Health 1973;27(5):312–7.

[35] Luo S, Liu X, Mu S, Tsai SP, Wen CP. Asbestos related diseases from environmental exposure to crocidolite in Da-yao, China. I. Review of exposure and epidemiological data. Occup Environ Med 2003;60(1):35–42.

[36] McDonald JC, McDonald AD. The epidemiology of mesothelioma in historical context. Eur Respir J 1996;9(9):1932–42.

[37] Selikoff IJ, Lilis R, Nicholson WJ. Asbestos disease in United States shipyards. Ann N Y Acad Sci 1979;330:295–311.

Silica and titanium dioxide nanoparticles cause pregnancy complications in mice

Kohei Yamashita[1,2†], Yasuo Yoshioka[1,2,3†]★, Kazuma Higashisaka[1,2], Kazuya Mimura[4], Yuki Morishita[1,2], Masatoshi Nozaki[4], Tokuyuki Yoshida[1,2], Toshinobu Ogura[1,2], Hiromi Nabeshi[1,2], Kazuya Nagano[2], Yasuhiro Abe[2], Haruhiko Kamada[2,3], Youko Monobe[5], Takayoshi Imazawa[5], Hisae Aoshima[6], Kiyoshi Shishido[7], Yuichi Kawai[8], Tadanori Mayumi[8], Shin-ichi Tsunoda[2,3,9], Norio Itoh[1], Tomoaki Yoshikawa[1,2], Itaru Yanagihara[4], Shigeru Saito[10] and Yasuo Tsutsumi[1,2,3]★

The increasing use of nanomaterials has raised concerns about their potential risks to human health. Recent studies have shown that nanoparticles can cross the placenta barrier in pregnant mice and cause neurotoxicity in their offspring, but a more detailed understanding of the effects of nanoparticles on pregnant animals remains elusive. Here, we show that silica and titanium dioxide nanoparticles with diameters of 70 nm and 35 nm, respectively, can cause pregnancy complications when injected intravenously into pregnant mice. The silica and titanium dioxide nanoparticles were found in the placenta, fetal liver and fetal brain. Mice treated with these nanoparticles had smaller uteri and smaller fetuses than untreated controls. Fullerene molecules and larger (300 and 1,000 nm) silica particles did not induce these complications. These detrimental effects are linked to structural and functional abnormalities in the placenta on the maternal side, and are abolished when the surfaces of the silica nanoparticles are modified with carboxyl and amine groups.

Nanomaterials such as nanosilica particles (nSPs), titanium dioxide nanoparticles (nano-TiO$_2$) and carbon nanotubes are already being applied in electronics[1], foods[2], cosmetics[3] and drug delivery[4]. nSPs are used as additives in cosmetics and foods because they are highly hydrophilic, easy to synthesize and their surfaces can be modified easily[5,6]. The increasing use of nanomaterials has raised concerns[7–9] because of recent reports showing that carbon nanotubes can induce mesothelioma-like lesions in mice, similar to those induced by asbestos[10,11]. We have also shown that nSPs can induce severe liver damage in mice and inflammatory responses in vitro[12,13].

Fetuses are known to be more sensitive to environmental toxins than adults[14–16], and it has been suggested that many chemical toxins in air, water and foods can induce pregnancy complications in humans[15,16]. An estimated 1 to 3% of women in the USA suffer recurrent miscarriages[17] and 7–15% of pregnancies are affected by poor fetal growth (a condition known as intrauterine growth restriction, IUGR)[18]. IUGR, which refers to a fetus with a weight below the 10th percentile for its gestational age, can cause fetal death and predisposes the child to a lifelong increased risk for cardiovascular disorders and renal disease[19,20]. Examining the potential risk of nanomaterials for causing miscarriage and IUGR is therefore essential.

Although some studies have shown transplacental transport of nanomaterials in pregnant animals and nanomaterial-induced neurotoxicity in their offspring[21–26], the effects of nanomaterials on pregnant animals have not yet been studied. Here, we investigated the biodistribution and fetotoxicity of various sizes of surface-modified nSPs, fullerene C$_{60}$ and nano-TiO$_2$ in pregnant mice. Our results indicate that nSPs with diameters less than 100 nm and nano-TiO$_2$ with diameters of 35 nm induce resorption of embryos and fetal growth restriction. Furthermore, we found that modifying the surface of nSPs from –OH to –COOH or –NH$_2$ functional groups can prevent these pregnancy complications. These data include basic information regarding possible ways of creating safer nanomaterials.

Biodistribution of nanoparticles

Silica particles are well suited for studying the influence of nanomaterial size on biodistribution and various biological effects because they show much better dispersibility in aqueous solutions than most other nanomaterials[27]. We used silica particles with diameters of 70 nm (nSP70), 300 nm (nSP300) and 1,000 nm (mSP1000) to study the effect of size on biodistribution of the particles in pregnant mice. Two other common nanomaterials, nano-TiO$_2$ and fullerene, were also examined. All silica nanoparticles were confirmed by transmission electron microscopy (TEM) to be smooth-surfaced spheres (Supplementary Fig. S1a,b,c,g,h,i)[12,13]. The hydrodynamic diameters of nSP70, nSP300, mSP1000, nano-TiO$_2$ and fullerene were 65, 322, 1,140, 217 and 143 nm, respectively, with zeta

[1]Department of Toxicology and Safety Science, Graduate School of Pharmaceutical Sciences, Osaka University, 1-6 Yamadaoka, Suita, Osaka 565-0871, Japan, [2]Laboratory of Biopharmaceutical Research, National Institute of Biomedical Innovation, 7-6-8, Saito-Asagi, Ibaraki, Osaka 567-0085, Japan, [3]The Center for Advanced Medical Engineering and Informatics, Osaka University, 1-6, Yamadaoka, Suita, Osaka 565-0871, Japan, [4]Department of Developmental Medicine, Osaka Medical Center and Research Institute for Maternal and Child Health, 840 Murodo-cho, Izumi, Osaka 594-1101, Japan, [5]Bioresources Research, Laboratory of Common Apparatus, National Institute of Biomedical Innovation, 7-6-8, Saito-Asagi, Ibaraki, Osaka 567-0085, Japan, [6]Vitamin C60 BioResearch Corporation, 1-3-19, Yaesu, Chuo-ku, Tokyo 103-0028, Japan, [7]Mitsubishi Corporation, 2-6-1, Marunouchi, Chiyoda-ku, Tokyo 100-8086, Japan, [8]Graduate School of Pharmaceutical Sciences, Kobe-Gakuin University, 1-1-3, Minatojima, Chuo-ku, Kobe, Hyogo 650-8586, Japan, [9]Department of Biomedical Innovation, Graduate School of Pharmaceutical Sciences, Osaka University, 7-6-8 Saito-asagi, Ibaraki, Osaka 567-0085, Japan, [10]Department of Obstetrics and Gynecology, University of Toyama, 2630, Sugitani, Toyama 930-0194, Japan; [†]These authors contributed equally to this work. ★e-mail: yasuo@phs.osaka-u.ac.jp; ytsutsumi@phs.osaka-u.ac.jp

potentials of −53, −62, −67, −23 and −13 mV, respectively (see Supplementary Fig S2 for the physicochemical properties of all the materials). The size distribution spectrum of each silica particle showed a single peak (Supplementary Fig. S1m), and the hydrodynamic diameter corresponded almost precisely to the primary particle size for each sample (Supplementary Figs S1m and S2), indicating that the silica particles used in this study were well-dispersed in solution.

We examined the relationship between particle size and biodistribution in the placenta by whole-body imaging analysis after intravenous injection (through the tail vein) of fluorescent DY-676-labelled nSP70, nSP300 or mSP1000 into pregnant mice at gestational day 16 (GD16). At 24 h post-injection, intense fluorescence was observed in the liver of all mice receiving the differently sized nanoparticles (Fig. 1a), suggesting that the accumulation of nanoparticles in the liver is independent of size. Fluorescence was seen in the placenta of mice treated with nSP70, but not in mice treated with nSP300 or mSP1000 (Fig. 1a). We confirmed that ~5% of fluorescent DY-676 dissociated from the silica particles after in vitro incubation in phosphate buffered saline (PBS) for 24 h at 37 °C (Supplementary Fig. S1n), and no fluorescence was detected in the placenta of mice treated with fluorescent DY-676 only (data not shown), indicating that the fluorescence observed in the mice was caused by silica particle accumulation in the tissues.

TEM analysis revealed that nSP70 (nanosized spherical black objects in Fig. 1b–g) were found in placental trophoblasts (Fig. 1b,c), fetal liver (Fig. 1d,e) and fetal brain (Fig. 1f,g). No particles were seen in the placenta, fetal liver or fetal brain of mice treated with nSP300 or mSP1000 (data not shown). These results suggest that the biodistribution of silica particles varied according to particle size, and that only the smaller nSP70 nanoparticles accumulated in the placenta and fetus. Similarly, nano-TiO$_2$ were found in placental trophoblasts (Fig. 1h,i), the fetal liver (Fig. 1j,k) and fetal brain (Fig. 1l,m) after intravenous injection into pregnant mice. We did not evaluate the biodistribution of fullerene C$_{60}$ because of the difficulty in detecting fullerene using TEM.

Recently, several reports have shown that some nanomaterials can penetrate mouse and ex vivo human placental tissue[25,28], and it is generally known that high-molecular-weight species (>1,000 Da) do not penetrate the placenta by passive diffusion. Thus, we speculated that nSP70 either directly injured the blood–placenta barrier or was actively transported through it, or both. Furthermore, nSP70 in the fetal circulation would have access to the fetal liver and brain, because the development of the blood–brain barrier in the fetal brain is incomplete[29].

Fetotoxicity of nanoparticles

To determine the fetotoxicity of nSP70, nSP300, mSP1000, nano-TiO$_2$ and fullerene in pregnant mice, we intravenously injected the particles (100 μl, 0.8 mg per mouse) into pregnant mice on two consecutive days, at GD16 and GD17, and measured the maternal blood biochemistry. None of the silica particles induced any significant changes in the levels of aspartate aminotransferase (AST), alanine aminotransferase (ALT) and blood urea nitrogen (BUN), and all parameters remained within the physiological range, indicating that the particles did not induce maternal liver and kidney damage at the administered doses (Supplementary Fig. S3). Blood pressure and heart rates among all groups of mice that received silica nanoparticles were similar and comparable to control animals receiving PBS (Supplementary Fig. S4). However, there was a significant increase in the number of granulocytes in nSP70-treated pregnant mice compared with control mice receiving PBS (Supplementary Fig. S5).

When compared to control mice, the maternal body weight of nSP70- and nano-TiO$_2$-treated mice decreased at GD17 and GD18, whereas those treated with nSP300, mSP1000 and fullerenes

did not show any changes (Fig. 2a). Mice that received nSP70 and nano-TiO$_2$ had 20% and 30% lower uterine weights (Fig. 2b,c), respectively, and significantly higher fetal resorption rates than control mice and those that received nSP300, mSP1000 particles or fullerene (Fig. 2d). nSP70- and nano-TiO$_2$-treated mice also had smaller fetuses (nearly 10% lower than control mice, Fig. 2e,g) and smaller amnion sacs than mice that received nSP300, mSP1000 or fullerene.

In contrast, the weights of placentae were the same among all groups of mice (Fig. 2f,h). When mice were injected with lower concentrations of nSP70 (0.2 and 0.4 mg per mouse), none of the above symptoms was observed; fetal resorption and growth restriction were seen only at the highest dose used (0.8 mg per mouse; Supplementary Fig. S6). These results indicate that only nSP70 at the highest concentration and nano-TiO$_2$ induced fetal resorption and restricted fetal growth; fullerene did not induce any pregnancy complications. The doses used here are typical of preclinical studies for drug delivery applications of silica particles, intravenously administered at several hundred milligrams per mouse[30]. In contrast, the most common route of nano-TiO$_2$ exposure to humans is through the skin (for example, through the application of nano-TiO$_2$-containing cosmetics) and some reports have suggested that nano-TiO$_2$ particles do not penetrate into living skin[31,32]. Therefore, we believe that nano-TiO$_2$ may not induce any pregnancy complications following topical application. Furthermore, we have confirmed that the nano-TiO$_2$ used in this study did not induce cellular toxicity and DNA damage in vitro (data not shown).

It is known that the surface properties of nanomaterials can influence biodistribution, inflammatory responses and cellular toxicity[27,33]. We examined the relationship between fetotoxicity and the surface properties of nSP70. The nSP70 was surface-modified with COOH or NH$_2$ functional groups (nSP70-C or nSP70-N, respectively), and both were confirmed by TEM to be smooth-surfaced spherical particles (Supplementary Fig. S1). The hydrodynamic diameters of the nSP70-C and nSP70-N were 70 and 72 nm, respectively, with zeta potentials of −76 and −29 mV, respectively, indicating that surface modification changed the surface charge of the particles (Supplementary Fig. S2).

As with nSP70, mice that were intravenously injected with DY-676-labelled nSP70-C and nSP70-N showed fluorescence in the placenta (Fig. 1a). TEM analysis revealed that nSP70-C and nSP70-N were found in placental trophoblasts (Fig. 1n,q), fetal liver (Fig. 1o,r) and fetal brain (Fig. 1p,s), indicating that the particles accumulated in the placenta and fetus. The maternal body weights of mice treated with nSP70-C or nSP70-N were the same as those observed for control mice (Fig. 2a). nSP70-C and nSP70-N did not affect the uterine weight (Fig. 2c), fetal weight (Fig. 2e,g) or fetal resorption rate (Fig. 2b,d). These results suggest that modifying the surface of nSP70 can prevent resorption and fetal growth restriction induced by nSP70.

Placental dysfunction in nSP70-treated mice

Normal placental development is required for embryonic growth, and placental dysfunction has been associated with miscarriage and fetal growth restriction[34,35]. The mature murine placenta consists of four layers: maternal decidua, trophoblast giant cell, spongiotrophoblast and labyrinth[34,35] (Fig. 3a). Maternal spiral arteries converge into canals between the trophoblast giant cells, and these canals pass through the spongiotrophoblast and labyrinth layers[34,35]. The exchange of respiratory gases, nutrients and waste takes place in the labyrinth layer between the fetal blood vessels and maternal blood sinuses[34,35].

To clarify the relationship between particle size, fetotoxicity and placental dysfunction, we examined the pathological histology of the placenta in nSP-treated mice using haematoxylin and eosin (H&E) staining (Fig. 3b–e). The placenta of mice treated with nSP70 showed variable structural abnormalities, whereas those treated
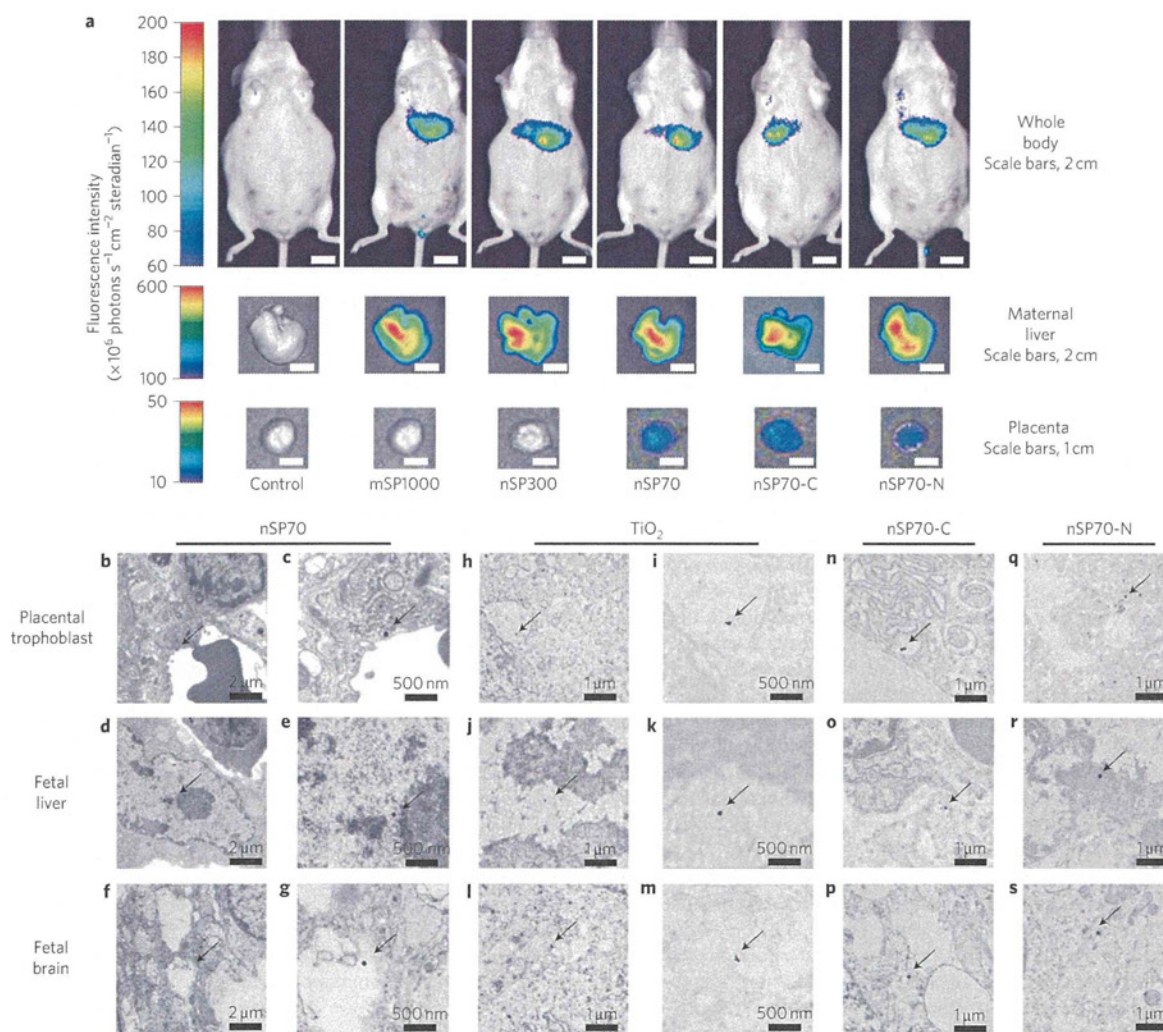
Figure 1 | Biodistribution of nanoparticles in pregnant mice. a, *In vivo* fluorescence images. Pregnant mice at GD16 were treated with 0.8 mg DY-676-labelled silica particles per mouse (nSP70, nSP300, mSP1000, nSP70-C or nSP70-N) or PBS (control), intravenously, through the tail vein. After 24 h, optical images of the whole body, maternal liver and placenta were acquired with a Xenogen IVIS 200 imaging system. **b–s**, TEM images of placentae and fetuses at GD18. Pregnant mice were treated intravenously with 0.8 mg per mouse of nSP70, nano-TiO$_2$, nSP70-C or nSP70-N on two consecutive days (GD16 and GD17). Arrows indicate nanoparticles. These particles were present in placental trophoblast cells (**b,c,h,i,n,q**), fetal liver cells (**d,e,j,k,o,r**) and fetal brain cells (**f,g,l,m,p,s**).

with nSP300 and mSP1000 did not show any significant abnormalities when compared to control mice (Fig 3b,d). Spiral artery canals failed to form (Fig. 3b,d) and blood flow was reduced in the fetal vascular sinuses of nSP70-treated mice (Fig. 3c,e). To further elucidate the influence of nanoparticles on placental dysfunction, we are examining the pathological histology of the placenta in nano-TiO$_2$-treated mice at present.

The areas including the placental major layers (the spongiotrophoblast and labyrinth) in nSP70-treated and control mice were examined by periodic acid–Schiff (PAS) staining (Fig. 3f–i). The total areas of placentae from each nSP70-treated mouse were not significantly different from those of control mice (Fig. 4a). The area of the spongiotrophoblast layer (Fig. 4b) and the ratio of the spongiotrophoblast layer area to the total placental area (Fig. 4c) in nSP70-treated mice were almost 50% smaller than those observed in control mice. The percentage of nuclei positively stained by terminal transferase-mediated dUTP nick end-labelling (TUNEL) was significantly higher within the spongiotrophoblast layer of

nSP70-treated mice than within that of control mice, indicating that nSP70 induced apoptotic cell death of spongiotrophoblasts (Fig. 3j,k; Fig. 4d). The surrounding lengths of the villi in the labyrinth layer of nSP70-treated mice were significantly decreased compared to those of control mice (Fig. 3l,m; Fig. 4f), whereas the ratio of the labyrinth layer area to the total placental area in nSP70-treated mice was not significantly different from that of control mice (Fig. 4e). These results suggest that nSP70-induced pregnancy complications were probably caused by placental cellular damage, which might affect maternal–fetal exchange.

Normal placental development requires the coordinated expression of vascular endothelial growth factor (VEGF) and its receptor, fms-like tyrosine kinase-1 (Flt-1)[36]. Soluble Flt-1 (sFlt-1) is expressed by placental cells including spongiotrophoblasts, and is a potent anti-angiogenic molecule that regulates the generation of placental vasculature during pregnancy by sequestering circulating VEGF and regulating the action of VEGF[37]. The plasma level of sFlt-1 in nSP70- and nano-TiO$_2$-treated mice was significantly
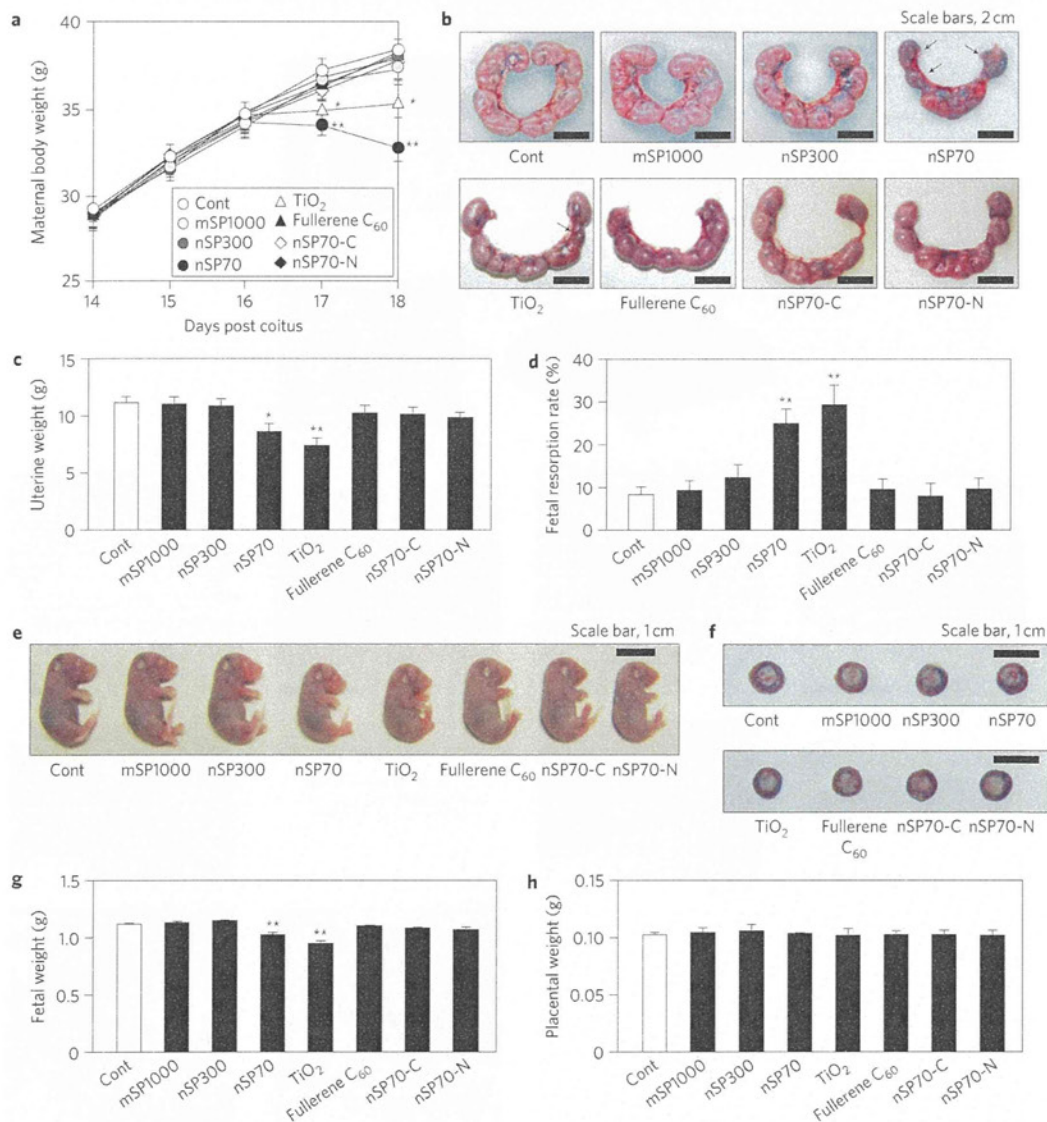
Figure 2 | Pregnancy complications in nSP70- or nano-TiO$_2$-treated mice. Pregnant mice were treated intravenously with 0.8 mg per mouse of nSP70, nSP300, mSP1000, nano-TiO$_2$, fullerene C$_{60}$, nSP70-C, nSP70-N or PBS (control) on two consecutive days (GD16 and GD17). **a**, Changes in maternal body weight. Maternal body weights were evaluated daily (n = 11–24). Statistically significant difference from control mice, *P < 0.05 and **P < 0.01 by ANOVA. **b–h**, Pregnancy complications. Uteri from mice were excised at GD18 (**b**). Uterine weights (**c**) and fetal resorption rates (**d**) were evaluated (n = 11–24). Fetuses (**e**) and placentae (**f**) were excised from uteri. Fetal weights (**g**) and placental weights (**h**) were evaluated (n = 37–212). All data represent means ± s.e.m (*P < 0.05, **P < 0.01 versus value for control mice by ANOVA).

lower than in control mice and those receiving nSP300, mSP1000, fullerene, nSP70-C and nSP70-N (Supplementary Fig. S7a–d), indicating that nSP70 induced not only structural abnormalities, but also functional abnormalities, in the mouse placenta.

The anticoagulation agent heparin is often administered to prevent miscarriage and IUGR[38]. Mice treated with a combination of nSP70 and heparin had slightly increased maternal body weights and decreased fetal resorption rates compared to mice that were not treated with heparin (Fig. 5a,c). Heparin treatment prevented decreases in uterine and fetal weight in nSP70-treated mice (Fig. 5b,d). Mice treated with a combination of nSP70 and heparin had similar levels of sFlt-1 to control mice (Supplementary Fig. S7e). These results suggest that the mechanism for nSP70-induced pregnancy complications might involve coagulation. However, it has recently been shown that heparin acts in

many ways other than as an anticoagulant[39–42]. The anti-complement activation effect of heparin has been suggested to be important in mitigating pregnancy complications[40]. Complement activation induces neutrophil activation and this may lead to placental dysfunction, miscarriage, fetal growth restriction or pre-eclampsia[43,44]. Here, we have shown that the number of granulocytes in nSP70-treated mice is significantly higher than in control mice (Supplementary Fig. S5), indicating that nSP70 might have induced complement activation, which may have subsequently activated neutrophils and systemic inflammation.

Some reports have shown that heparin may also act as a placental growth factor, because heparin is known to inhibit placental apoptosis, stimulate placental proliferation and enhance the effect of several growth factors[39,41,42]. Moreover, oxidative stress in the placenta is known to cause placental dysfunction and to induce pregnancy
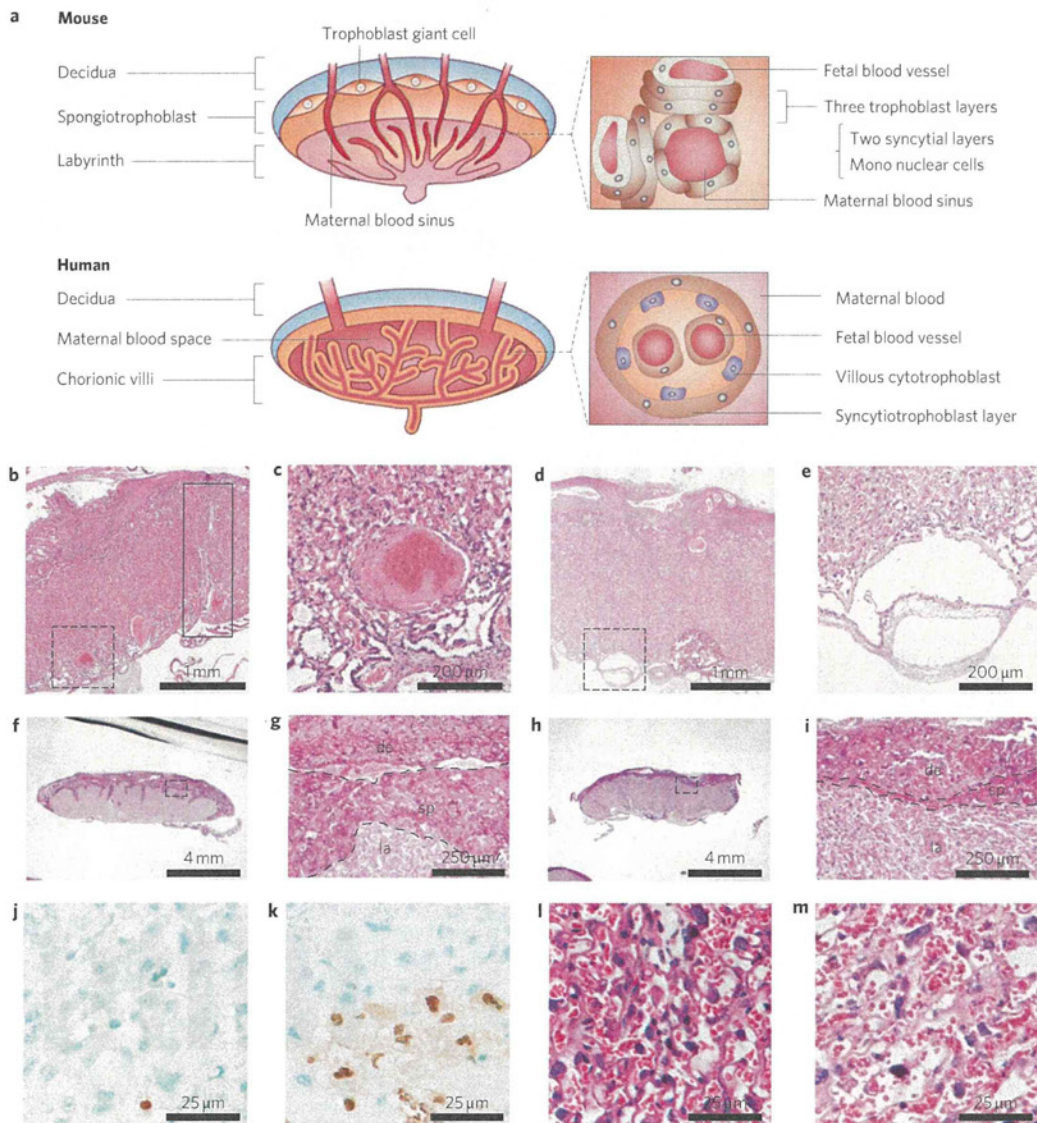
Figure 3 | Pathological examination of placenta. a, Schematic showing the differences between human and mouse placentae. **b–m**, Histological examination. Pregnant mice were treated intravenously with 0.8 mg per mouse of nSP70 or PBS (control) on two consecutive days (GD16 and GD17). At GD18, sections of placentae from PBS- (**b,c,f,g**) or nSP70-treated mice (**d,e,h,i**) were stained with H&E (**b–e**) or PAS (**f–i**). The solid box in **b** indicates the presence of spiral arteries and canals. Panels **c, e, g,** and **i** are enlarged images of the areas within the dashed boxes in **b, d, f** and **h**, respectively. In **g** and **i**, dashed lines delineate the decidua (de), spongiotrophoblast layer (sp) and labyrinth layer (la). Spongiotrophoblast layers of PBS- (**j**) or nSP70-treated mice (**k**) were stained with TUNEL. Labyrinth layers of PBS- (**l**) or nSP70-treated mice (**m**) were stained with H&E.

complications[45]. Nanomaterials have been reported to cause oxidative stress, which in turn induces cell apoptosis and inflammation[22,46,47]. Therefore, the pregnancy complications observed here might have been caused by oxidative stress induced by nSP70.

We have observed that the induction of oxidative stress in cells and the activation of the coagulation pathway in mice treated with nSP70-C and nSP70-N were lower than those observed in cells and mice treated with nSP70 (unpublished data). Therefore, we speculate that the lower activation of coagulation, complement and oxidative stress in the placenta of mice treated with nSP70-C and nSP70-N might have prevented pregnancy complications in those mice. It has recently been shown that nanomaterials become coated with serum proteins and induce different cellular responses by binding to proteins[48]. In addition, different surface characteristics, such as surface charge, are known to influence the binding affinities of

proteins to nanomaterials[48]. Therefore, the differences in protein binding among nSP70, nSP70-C and nSP70-N might have given rise to differences in the fetotoxicity of the nanomaterials.

It should be noted that there are differences between mouse and human placentae, such as the greater role of yolk sac placentation in the mouse and the anatomy in the labyrinth[49,50] (Fig. 3a). The yolk sac plays a significant role in material transport from mother to fetus in mice, especially before the placental circulation is established[49]. Therefore, the accumulation of nSP70 in the yolk sac should be investigated to understand the accumulation mechanism of nanoparticles in fetuses. In the mouse placenta, three trophoblast layers embrace the fetal vasculature in the labyrinth layer, whereas in the human term placenta, a single syncytial layer with an underlying trophoblast stem cell layer is present in the villi[49,50]. As these anatomical and structural differences might affect nanoparticle
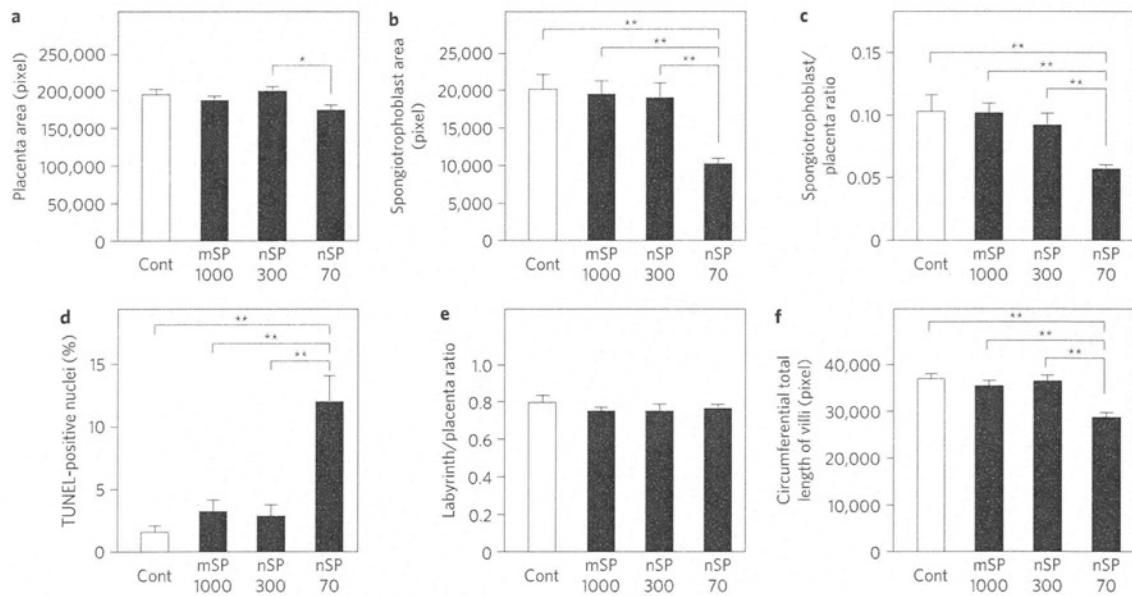
Figure 4 | Dysfunction of placentae. Pregnant mice were treated intravenously with 0.8 mg per mouse of nSP70, nSP300, mSP1000 or PBS (control) on two consecutive days (GD16 and GD17). **a–e**, At GD18, the area of the placenta (**a**) and the spongiotrophoblast layer (**b**) and the ratios of the spongiotrophoblast layer area to the total placental area (**c**) and of the labyrinth layer area to the total placental area (**e**) were assessed by examining the PAS-stained sections in Fig. 3f–i and were analysed quantitatively. The apoptotic index (**d**) was assessed by examining the TUNEL-stained sections in Fig. 3j,k and was quantitatively analysed. The surrounding length of the villi (**f**) in the labyrinth layers was assessed by examining the H&E-stained sections in Fig. 3l,m and was quantitatively analysed. All data represent means ± s.e.m. ($n = 11$–20; $*P < 0.05$ and $**P < 0.01$ by ANOVA).
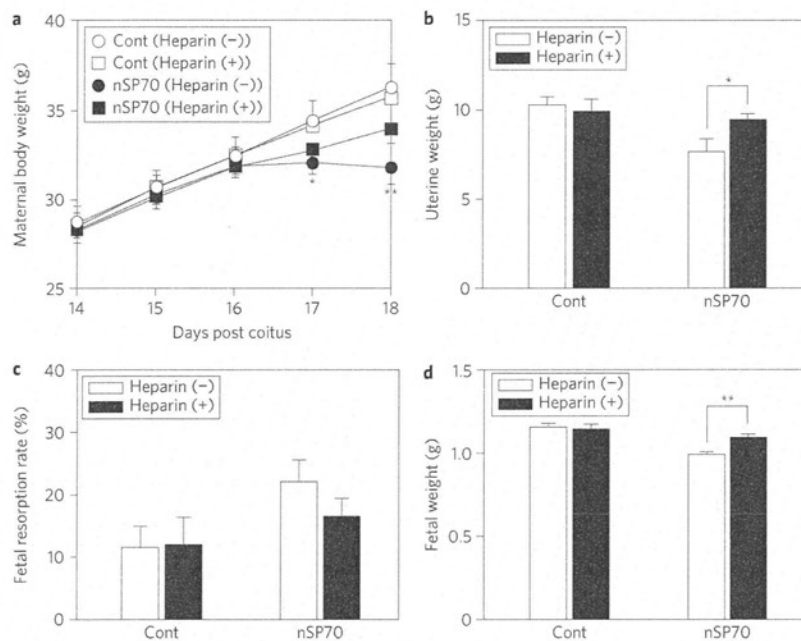

Figure 5 | Prevention of nSP70-induced pregnancy complications with heparin. Pregnant mice were treated intravenously with 0.8 mg per mouse of nSP70 or PBS (control) through the tail vein with or without heparin on two consecutive days (GD16 and GD17). **a**, Changes in maternal body weights. Maternal body weights were evaluated daily ($n = 10$–15). Statistically significant difference from control mice, $*P < 0.05$ and $**P < 0.01$ by ANOVA. **b–d**, Analysis of pregnancy complications in nSP70-treated mice with or without heparin treatment. At GD18, uterine weights (**b**), fetal resorption rates (**c**) and fetal weights (**d**) were evaluated (**b,c**, $n = 10$–15; **d**, $n = 55$–89). All data represent means ± s.e.m., $*P < 0.05$ and $**P < 0.01$ by Student's t-tests.

uptake and distribution, we cannot extrapolate our data about the placental distribution of nanoparticles, or placental dysfunction induced by nanoparticles, to humans. Additional studies that examine the penetration efficiency of nanoparticles into the human placenta (using *ex vivo* human placental tissue) are needed, as are studies that focus on the relationship between pregnancy complications and the amount of nanoparticles in the human placenta.

Conclusion

Of the materials studied here, nSP70 and nano-TiO$_2$ induced fetal resorption and restricted the growth of fetuses in pregnant mice, whereas fullerene C$_{60}$ did not induce these complications. nSP70 and nano-TiO$_2$ were observed in the placenta, fetal liver and fetal brain, and nSP70 induced complications only at the highest concentration (0.8 mg per mouse) administered. The detrimental effects seen in nSP70-treated mice were linked to structural and functional changes in the placenta. Modification of the surface of nSP70 with carboxyl or amine groups abrogated the negative effects, suggesting the importance of surface charge. Although the nSP70 and nano-TiO$_2$ were mainly designed for experimental and industrial use, and not for cosmetics or food, we suggest that the potential fetotoxicity of these and other nanomaterials should be investigated more carefully.

Methods

Particles. nSP70, nSP300, mSP1000, nSP70-C and nSP70-N, as well as nSP70, nSP300 and mSP1000 labelled with DY-676 (excitation and emission wavelengths of 674 and 699 nm, respectively), were purchased from Micromod Partikeltechnologie. Rutile-type TiO$_2$ particles with a diameter of 35 nm (designated nano-TiO$_2$, Tayca Corporation) were also used. Polyvinylpyrrolidone (PVP)-wrapped fullerene C$_{60}$ was provided by Vitamin C60 BioResearch Corporation. The nanoparticles were used after 5 min of sonication (280 W output (Ultrasonic Cleaner, AS One) and 1 min of vortexing.

Mice. Pregnant BALB/c mice (8–10 weeks) were purchased from Japan SLC. The experimental protocols conformed to the ethical guidelines of Osaka University and the National Institute of Biomedical Innovation, Japan.

In vivo **imaging.** *In vivo* fluorescence imaging was performed with an IVIS 200 small-animal imaging system (Xenogen). At GD16, pregnant BALB/c mice were injected with 100 μl (0.8 mg per mouse) DY-676-labelled nSP70, nSP300, mSP1000, nSP70-C, nSP70-N or PBS (control), intravenously through the tail vein. At 24 h post-injection, the mice were anaesthetized, and images were obtained with a cy5.5 filter set (excitation/emission, 615–665 nm/695–770 nm). Imaging parameters were selected and implemented with Living Image 2.5 software (Xenogen).

TEM analysis. Pregnant BALB/c mice were treated with 100 μl (0.8 mg per mouse) of nSP70, nSP300, mSP1000, nSP70-C, nSP70-N or nano-TiO$_2$, intravenously through the tail vein, on two consecutive days (GD16 and GD17). At GD18, mice were killed after being anaesthetized, and the placenta, fetal liver and fetal brain were fixed in 2.5% glutaraldehyde for 2 h. Small pieces of tissue collected from these samples were washed with phosphate buffer, postfixed in sodium cacodylate-buffered 1.5% osmium tetroxide for 60 min at 4 °C, dehydrated using a series of ethanol concentrations, and embedded in Epon resin. The samples were examined under a Hitachi electron microscope (H-7650; Hitachi).

Fetotoxicity. Pregnant BALB/c mice were treated with 100 μl of nSP70 (0.2 mg, 0.4 mg or 0.8 mg per mouse), nSP300 (0.8 mg per mouse), mSP1000 (0.8 mg per mouse), nSP70-C (0.8 mg per mouse), nSP70-N (0.8 mg per mouse), nano-TiO$_2$ (0.8 mg per mouse), fullerene C$_{60}$ (0.8 mg per mouse) or PBS (control), intravenously through the tail vein, on two consecutive days (GD16 and GD17). All mice were killed after being anaesthetized at GD18. Blood samples were collected in tubes containing 5 IU ml^{-1} heparin sodium, and plasma was harvested. The rate of fetal resorption was calculated (number of resorptions/total number of formed fetuses and resorptions). The fetuses and placentae of each mouse were excised and weighed, and the weight of the uterus calculated as the sum of the placental and fetal weights. To study the effects of heparin in nSP70-treated mice, pregnant BALB/c mice were treated with 100 μl (0.8 mg per mouse) nSP70 or PBS (control) intravenously through the tail vein on two consecutive days (GD16 and GD17). The same mice were treated with heparin (Sigma-Aldrich, 10 U) intraperitoneally on two consecutive days (GD16 and GD17), twice a day, 3 h before nSP70 treatment and 3 h after nSP70 treatment.

Histological examination. After fixing placentae in 10% formalin neutral buffer solution overnight, tissues were washed in PBS, dehydrated in a graded series of ethanol and xylene solutions, and embedded in paraffin. Sections (2 μm) were cut with a microtome. Sections were deparaffinized, rehydrated in a graded series of ethanols, and stained with H&E or PAS. Stained sections were dehydrated in a series of ethanols and mounted using permount. Representative histological images were recorded with a charge-coupled device (CCD) digital camera fixed to a microscope. The areas of the placenta, spongiotrophoblast layer and labyrinth layer were assessed by examining light microscopy images (Olympus) of the PAS-stained sections and were quantitatively analysed with Image J Imaging System Software Version 1.3 (National Institutes of Health). The circumferential total length of villi was assessed by examining light microscopy images of the H&E-stained sections and quantitatively analysed with Image J Imaging System Software Version 1.3. The

presence of apoptotic cells in placental sections was analysed by TUNEL assay (Millipore). The tissue was counterstained with methyl green. Photographs of TUNEL (brown) and methyl green (light blue) staining were captured at three randomly selected fields in the spongiotrophoblast layer. TUNEL-positive nuclei (apoptotic nuclei) and methyl green-stained nuclei (total nuclei) were counted in the spongiotrophoblast layer. The apoptotic index in each section was calculated as the percentage of spongiotrophoblast nuclei stained TUNEL-positive divided by the total number of methyl green-stained nuclei found within the spongiotrophoblast layer.

References

1. Konstantatos, G. & Sargent, E. H. Nanostructured materials for photon detection. *Nature Nanotech.* **5,** 391–400 (2010).
2. Augustin, M. A. & Sanguansri, P. Nanostructured materials in the food industry. *Adv. Food. Nutr. Res.* **58,** 183–213 (2009).
3. Bowman, D. M., van Calster, G. & Friedrichs, S. Nanomaterials and regulation of cosmetics. *Nature Nanotech.* **5,** 92 (2010).
4. Petros, R. A. & DeSimone, J. M. Strategies in the design of nanoparticles for therapeutic applications. *Nature Rev. Drug Discov.* **9,** 615–627 (2010).
5. Martin, K. R. The chemistry of silica and its potential health benefits. *J. Nutr. Health Aging.* **11,** 94–97 (2007).
6. Knopp, D., Tang, D. & Niessner, R. Review: bioanalytical applications of biomolecule-functionalized nanometer-sized doped silica particles. *Anal. Chim. Acta.* **647,** 14–30 (2009).
7. Kagan, V. E., Bayir, H. & Shvedova, A. A. Nanomedicine and nanotoxicology: two sides of the same coin. *Nanomedicine* **1,** 313–316 (2005).
8. Nel, A., Xia, T., Madler, L. & Li, N. Toxic potential of materials at the nanolevel. *Science* **311,** 622–627 (2006).
9. Fadeel, B. & Garcia-Bennett, A. E. Better safe than sorry: understanding the toxicological properties of inorganic nanoparticles manufactured for biomedical applications. *Adv. Drug. Deliv. Rev.* **62,** 362–374 (2010).
10. Poland, C. A. *et al.* Carbon nanotubes introduced into the abdominal cavity of mice show asbestos-like pathogenicity in a pilot study. *Nature Nanotech.* **3,** 423–428 (2008).
11. Donaldson, K., Murphy, F. A., Duffin, R. & Poland, C. A. Asbestos, carbon nanotubes and the pleural mesothelium: a review of the hypothesis regarding the role of long fibre retention in the parietal pleura, inflammation and mesothelioma. *Part. Fibre Toxicol.* **7,** 5 (2010).
12. Nabeshi, H. *et al.* Systemic distribution, nuclear entry and cytotoxicity of amorphous nanosilica following topical application. *Biomaterials* **32,** 2713–2724 (2011).
13. Nabeshi, H. *et al.* Amorphous nanosilica induce endocytosis-dependent ROS generation and DNA damage in human keratinocytes. *Part. Fibre Toxicol.* **8,** 1 (2011).
14. Koren, G., Pastuszak, A. & Ito, S. Drugs in pregnancy. *N. Engl. J. Med.* **338,** 1128–1137 (1998).
15. Tardiff, R. G., Carson, M. L. & Ginevan, M. E. Updated weight of evidence for an association between adverse reproductive and developmental effects and exposure to disinfection by-products. *Regul. Toxicol. Pharmacol.* **45,** 185–205 (2006).
16. Wigle, D. T. *et al.* Epidemiologic evidence of relationships between reproductive and child health outcomes and environmental chemical contaminants. *J. Toxicol. Environ. Health. B. Crit. Rev.* **11,** 373–517 (2008).
17. Mills, J. L. *et al.* Incidence of spontaneous abortion among normal women and insulin-dependent diabetic women whose pregnancies were identified within 21 days of conception. *N. Engl. J. Med.* **319,** 1617–1623 (1988).
18. Cetin, I. & Alvino, G. Intrauterine growth restriction: implications for placental metabolism and transport. A review. *Placenta* **30(Suppl. A),** S77–S82 (2009).
19. Godfrey, K. M. & Barker, D. J. Fetal nutrition and adult disease. *Am. J. Clin. Nutr.* **71,** 1344S–1352S (2000).
20. Barker, D. J. Adult consequences of fetal growth restriction. *Clin. Obstet. Gynecol.* **49,** 270–283 (2006).
21. Takeda, K. *et al.* Nanoparticles transferred from pregnant mice to their offspring can damage the genital and cranial nerve systems. *J. Health Sci.* **55,** 95–102 (2009).
22. Shimizu, M. *et al.* Maternal exposure to nanoparticulate titanium dioxide during the prenatal period alters gene expression related to brain development in the mouse. *Part. Fibre Toxicol.* **6,** 20 (2009).
23. Tian, F. *et al.* Surface modification and size dependence in particle translocation during early embryonic development. *Inhal. Toxicol.* **21(Suppl. 1),** 92–96 (2009).
24. Saunders, M. Transplacental transport of nanomaterials. *Wiley Interdiscip. Rev. Nanomed. Nanobiotechnol.* **1,** 671–684 (2009).

25. Chu, M. *et al.* Transfer of quantum dots from pregnant mice to pups across the placental barrier. *Small* **6**, 670–678 (2010).
26. Hougaard, K. S. *et al.* Effects of prenatal exposure to surface-coated nanosized titanium dioxide (UV-Titan). A study in mice. *Part. Fibre Toxicol.* **7**, 16 (2010).
27. He, X. *et al. In vivo* study of biodistribution and urinary excretion of surface-modified silica nanoparticles. *Anal. Chem.* **80**, 9597–9603 (2008).
28. Wick, P. *et al.* Barrier capacity of human placenta for nanosized materials. *Environ. Health Perspect.* **118**, 432–436 (2010).
29. Watson, R. E., Desesso, J. M., Hurtt, M. E. & Cappon, G. D. Postnatal growth and morphological development of the brain: a species comparison. *Birth Defects Res. B. Dev. Reprod. Toxicol.* **77**, 471–484 (2006).
30. Li, L. *et al. In vivo* delivery of silica nanorattle encapsulated docetaxel for liver cancer therapy with low toxicity and high efficacy. *ACS Nano.* **4**, 6874–6882 (2010).
31. Filipe, P. *et al.* Stratum corneum is an effective barrier to TiO_2 and ZnO nanoparticle percutaneous absorption. *Skin Pharmacol. Physiol.* **22**, 266–275 (2009).
32. Sadrieh, N. *et al.* Lack of significant dermal penetration of titanium dioxide from sunscreen formulations containing nano- and submicron-size TiO_2 particles. *Toxicol. Sci.* **115**, 156–166 (2010).
33. Albrecht, C. *et al.* Inflammatory time course after quartz instillation: role of tumor necrosis factor-alpha and particle surface. *Am. J. Respir. Cell. Mol. Biol.* **31**, 292–301 (2004).
34. Kibschull, M., Gellhaus, A. & Winterhager, E. Analogous and unique functions of connexins in mouse and human placental development. *Placenta* **29**, 848–854 (2008).
35. Gasperowicz, M. & Otto, F. The notch signalling pathway in the development of the mouse placenta. *Placenta* **29**, 651–659 (2008).
36. Lam, C., Lim, K. H. & Karumanchi, S. A. Circulating angiogenic factors in the pathogenesis and prediction of preeclampsia. *Hypertension* **46**, 1077–1085 (2005).
37. Hirashima, M., Lu, Y., Byers, L. & Rossant, J. Trophoblast expression of fms-like tyrosine kinase 1 is not required for the establishment of the maternal–fetal interface in the mouse placenta. *Proc. Natl Acad. Sci. USA* **100**, 15637–15642 (2003).
38. Derksen, R. H., Khamashta, M. A. & Branch, D. W. Management of the obstetric antiphospholipid syndrome. *Arthritis Rheum.* **50**, 1028–1039 (2004).
39. Li, Y., Wang, H. Y. & Cho, C. H. Association of heparin with basic fibroblast growth factor, epidermal growth factor, and constitutive nitric oxide synthase on healing of gastric ulcer in rats. *J. Pharmacol. Exp. Ther.* **290**, 789–796 (1999).
40. Girardi, G., Redecha, P. & Salmon, J. E. Heparin prevents antiphospholipid antibody-induced fetal loss by inhibiting complement activation. *Nature Med.* **10**, 1222–1226 (2004).
41. Hills, F. A. *et al.* Heparin prevents programmed cell death in human trophoblast. *Mol. Hum. Reprod.* **12**, 237–243 (2006).
42. Hossain, N., Schatz, F. & Paidas, M. J. Heparin and maternal fetal interface: why should it work to prevent pregnancy complications? *Thromb. Res.* **124**, 653–655 (2009).
43. Girardi, G., Yarilin, D., Thurman, J. M., Holers, V. M. & Salmon, J. E. Complement activation induces dysregulation of angiogenic factors and causes fetal rejection and growth restriction. *J. Exp. Med.* **203**, 2165–2175 (2006).
44. Redecha, P., van Rooijen, N., Torry, D. & Girardi, G. Pravastatin prevents miscarriages in mice: role of tissue factor in placental and fetal injury. *Blood* **113**, 4101–4109 (2009).
45. Myatt, L. & Cui, X. Oxidative stress in the placenta. *Histochem. Cell. Biol.* **122**, 369–382 (2004).
46. Hussain, S. *et al.* Oxidative stress and proinflammatory effects of carbon black and titanium dioxide nanoparticles: role of particle surface area and internalized amount. *Toxicology* **260**, 142–149 (2009).
47. Liu, X. & Sun, J. Endothelial cells dysfunction induced by silica nanoparticles through oxidative stress via JNK/P53 and NF-κB pathways. *Biomaterials* **31**, 8198–8209 (2010).
48. Lundqvist, M. *et al.* Nanoparticle size and surface properties determine the protein corona with possible implications for biological impacts. *Proc. Natl Acad. Sci. USA* **105**, 14265–14270 (2008).
49. Enders, A. C. & Blankenship, T. N. Comparative placental structure. *Adv. Drug Deliv. Rev.* **38**, 3–15 (1999).
50. Rossant, J. & Cross, J. C. Placental development: lessons from mouse mutants. *Nature Rev. Genet.* **2**, 538–548 (2001).

Author contributions

K.Y. and Y.Y. designed the study. K.Y., K.H., K.M., Y. Morishita, M.N., T. Yoshida, T.O., H.N., K.N., Y.A., H.K., Y. Monobe and T.I. performed the experiments. K.Y. and Y.Y. collected and analysed the data. K.Y. and Y.Y. wrote the manuscript. H.A., K.S., Y.K., T.M., S.T., N.I., I.Y., S.S. and T. Yoshikawa provided technical support and conceptual advice. Y.T. supervised the project. All authors discussed the results and commented on the manuscript.

Additional information

○ Nanoscale Research Letters
a SpringerOpen Journal

NANO EXPRESS

Open Access

Effect of surface properties of silica nanoparticles on their cytotoxicity and cellular distribution in murine macrophages

Hiromi Nabeshi[1,2], Tomoaki Yoshikawa[1,2*], Akihiro Arimori[1,2], Tokuyuki Yoshida[1,2], Saeko Tochigi[1,2], Toshiro Hirai[1,2], Takanori Akase[1,2], Kazuya Nagano[2], Yasuhiro Abe[2], Haruhiko Kamada[2,3], Shin-ichi Tsunoda[2,4], Norio Itoh[1], Yasuo Yoshioka[2,3], Yasuo Tsutsumi[1,2,3*]

Abstract

Surface properties are often hypothesized to be important factors in the development of safer forms of nanomaterials (NMs). However, the results obtained from studying the cellular responses to NMs are often contradictory. Hence, the aim of this study was to investigate the relationship between the surface properties of silica nanoparticles and their cytotoxicity against a murine macrophage cell line (RAW264.7). The surface of the silica nanoparticles was either unmodified (nSP70) or modified with amine (nSP70-N) or carboxyl groups (nSP70-C). First, the properties of the silica nanoparticles were characterized. RAW264.7 cells were then exposed to nSP70, nSP70-N, or nSP70-C, and any cytotoxic effects were monitored by analyzing DNA synthesis. The results of this study show that nSP70-N and nSP70-C have a smaller effect on DNA synthesis activity by comparison to unmodified nSP70. Analysis of the intracellular localization of the silica nanoparticles revealed that nSP70 had penetrated into the nucleus, whereas nSP70-N and nSP70-C showed no nuclear localization. These results suggest that intracellular localization is a critical factor underlying the cytotoxicity of these silica nanoparticles. Thus, the surface properties of silica nanoparticles play an important role in determining their safety. Our results suggest that optimization of the surface characteristics of silica nanoparticles will contribute to the development of safer forms of NMs.

Introduction

Recently, a range of nanomaterials (NMs) have been designed and used in a number of different industrial applications, such as medicine, cosmetics, and foods. The application of NMs is driven by the belief that they will offer improved performance and deliver new functionalities, including improved thermal and electrical conductivity, harder and stronger materials, improved catalytic activity, and advanced optical properties. For example, current estimates indicate that the global market for cosmetics using NMs will grow by 16.6% per year, reaching US$ 155.8 million in 2012 [1]. Hence, human exposure to NMs is already occurring and will inevitably increase in the future.

A NM is defined as a substance that has at least one dimension of <100 nm in size. NMs can assume many different forms, such as tubes, rods, wires, spheres, or particles. However, their small size can also be problematic in terms of eliciting a toxicological effect. For example, exposure of cells or animals to carbon nanotubes, titanium dioxide particles, or silver nanoparticles can induce cytotoxicity and inflammation [2-14]. We have previously shown that silica nanoparticles display a different intracellular localization compared with submicron- and micro-sized silica particles, and induce a greater cytotoxic response [15]. However, analyses of the toxicological responses to NMs are often inconsistent. Given the uncertainty concerning the safety of NMs, it is critically important to analyze their potential toxicological hazards and devise means of minimizing the impact of exposure to such substances. These studies will assist in driving forward the nanotechnology

∘* Correspondence: tomoaki@phs.osaka-u.ac.jp; ytsutsumi@phs.osaka-u.ac.jp
[1]Department of Toxicology and Safety Science, Graduate School of Pharmaceutical Sciences, Osaka University, 1-6 Yamadaoka, Suita, Osaka 565-0871, Japan
Full list of author information is available at the end of the article

industry in the longer term by helping the researchers to protect both individuals and the environment from potentially damaging materials.

Some recent articles have focused on the possible influence of surface charge in terms of the cellular uptake and/or cytotoxicity of nanoparticles [16-19]. Mayer et al. [19] reported the activation of the complement system and increased hemolysis in blood samples after exposure to positively charged polystyrene nanoparticles. Some recent studies suggest that cationic nanoparticles elicit a greater cytotoxicity compared with anionic nanoparticles [20-22]. Taken together, these studies indicate that the surface property of nanoparticles is an important factor when developing safer forms of NMs. However, studies of cellular responses to NMs often give conflicting results. The aim of this study was to investigate the cytotoxicity caused by exposure of a murine macrophage cell line (RAW264.7) to silica nanoparticles whose surface was either unmodified (nSP70) or modified with amine (nSP70-N) or carboxyl groups (nSP70-C). The intracellular localization of the different nanoparticles was also examined.

Experimental procedures
Silica particles
Fluorescent (red-F or green-F)-labeled silica particles with surfaces that were either unmodified or modified with amine or carboxyl groups (Micromod Partikeltechnologie GmbH, Rostock, Germany; designated nSP70, nSP70-N, and nSP70-C, respectively) were used in this study. The silica particles, which had a diameter of 70 nm, were prepared as a suspension (25 mg/ml) and sonicated for 5 min and then vortexed for 1 min immediately prior to conducting each experiment.

Physicochemical examination of the nanosilica preparations
Nanosilicas were diluted to 0.25 mg/ml with water, and the average particle size and zeta potential were measured using a Zetasizer Nano-ZS (Malvern Instruments Ltd., Malvern, UK). The mean size and the size distribution of silica particles were measured by dynamic light scattering. The zeta potential was measured by laser Doppler electrophoresis.

Cell culture
The mouse macrophage cell line, RAW 264.7, was obtained from the American Type Culture Collection. RAW 264.7 cells were cultured in Dulbecco's Modified Eagle Medium supplemented with 10% heat-inactivated FCS, 1% Antibiotic-Antimycotic Mix stock solution (GIBCO, CA, USA). All cultures were incubated at 37°C in a humidified atmosphere with 5% CO_2.

^{3}H-Thymidine incorporation assay
The proliferation of nanosilica-treated RAW 264.7 cells and untreated cells was measured using a ^{3}H-thymidine incorporation assay. 10^4 cells were cultured with varying concentrations of nanosilica diluted with medium for 18 h at 37°C, and ^{3}H-thymidine (1 μCi/well) was then added into each well. After a further 6 h, cells were harvested and lysed on glass fiber filter plates using a Cell harvester (Perkin-Elmer, Wellesley, MA, USA). The filter plates were then dried and counted by standard liquid scintillation counting techniques in a TopCounter (Perkin-Elmer).

Confocal scanning laser microscopy analysis of the macrophage cell line
RAW 264.7 cells were cultured with nSP70, nSP70-N, and nSP70-C (100 μg/ml) for 3 h on chamber slides, then fixed at room temperature in 4% paraformaldehyde and washed three times in 0.1 M phosphate buffer (pH 7.4). Cells were then filled with mounting medium containing 4',6-diamino-2-phenylindole (DAPI) (Vector Laboratories, Burlingame, CA, USA). A glass cover slip was then placed on the slide and fixed with glue. The mounted slides were examined under a confocal scanning laser microscope (Leica Microsystems, Mannheim, Germany).

Results and discussion
First, the authors assessed the mean particle size and surface charge of 70 nm silica particles in water whose surface was unmodified (nSP70) or chemically modified with amine (nSP70-N) or carboxyl groups (nSP70-C). The results are summarized in Table 1. Mean particle sizes of nSP70, nSP70-N, and nSP70-C as measured by dynamic light scattering method were 64.2 ± 0.6, 72.7 ± 1.3, and 76.2 ± 1.6 nm, respectively. These experimentally determined particle sizes were almost equal to the primary diameter sizes (70 nm). Surface charges (zeta potential) of nSP70-N and nSP70-C were, respectively, higher and lower compared to those of nSP70.

Cytotoxicity of the three nanosilicas was tested by monitoring the incorporation of ^{3}H-thymidine into RAW 264.7 cells. nSP70 showed the highest cytotoxicity (EC50 value = 121.5 μg/ml), while nSP70-N and nSP70-

Table 1 Average particle size and zeta potential of unmodified and modified nanosilica

	nSP70	nSP70-N	nSP70-C
Modification substance	-	NH_2	COOH
Mean particle size in water (nm)	64.2 ± 0.6	72.7 ± 1.3	76.2 ± 1.6
Mean zeta potential (mV)	-42.1 ± 0.6	-29.8 ± 0.5	-72.0 ± 1.9

Each value represents the mean ± SD.

C failed to display any detectable cytotoxicity up to concentrations of 1000 μg/ml (Figure 1). These results demonstrate that the cytotoxic effect of nSP70 is reduced by surface modification. Some reports indicated that the exposure of cells to silica nanoparticles leads to membrane damage, caspase activation, and cell death via apoptosis. The precise trigger for these silica nanoparticle-induced cellular effects is uncertain. One study concluded that lysosomal destabilization was the initiation factor [23], whereas other investigations suggest that mitochondrial membrane damage is the critical event [24,25]. However, it is possible that multiple factors (i.e., membrane damage, caspase activation, lysosomal destabilization, and mitochondrial membrane damage) are involved in nSP70-mediated cytotoxicity. Unfortunately, it is difficult to establish a comprehensive mechanism of nSP70 cytotoxicity based on previous observations, which have been rather inconsistent.

Some reports indicate that the cellular uptake and trafficking of nanoparticles is involved in cellular signaling, which then leads to cytotoxicity. However, the relationship between the surface properties of nanoparticles and cellular uptake/trafficking is poorly understood.

To establish why a different biological effect was induced by surface modification, the intracellular localization of fluorescent-labeled nanosilicas was investigated. RAW 264.7 cells treated with 100 μg/ml of nSP70, nSP70-N, and nSP70-C were observed by confocal laser scanning microscopy. After 3-h incubation, all nanosilicas were found to be localized in the cytoplasm as punctate fluorescent dots regardless of surface modification (Figure 2). Interestingly, distinctive distributions were observed in individual cases. For the nSP70-treated cells, punctate fluorescence was observed in both the cytoplasm and nucleus. However, nSP70-N appeared to adsorb to the plasma membrane because bright fluorescence was observed along the outline of the cell. In the nSP70-C-treated group, only intracellular punctate fluorescence was observed, suggesting that these particles were efficiently incorporated into the cells. Unfortunately, detailed intracellular localization of the silica nanoparticles was not apparent from these images. Nonetheless, differences of intracellular localization of nanosilica might have an effect on cytotoxicity. It is reported that the entry of nanosilica into the nucleus induces dysfunction of the nucleus and genotoxicity via
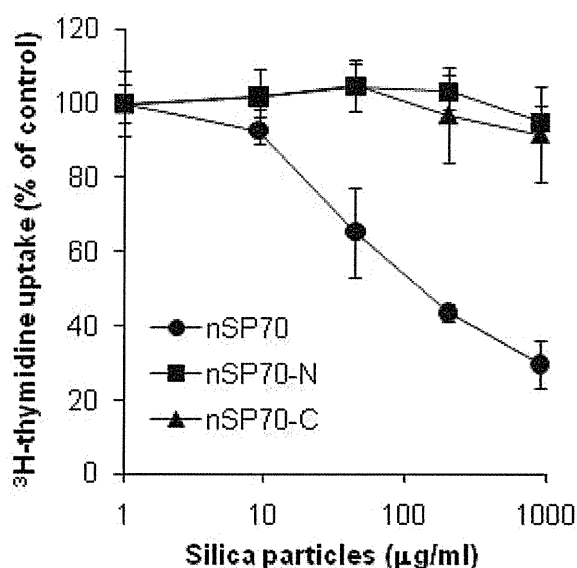

Figure 1 Effect of unmodified and modified nanosilica on cell proliferation. The proliferation of RAW 264.7 cells after incubation with nSP70 (circle), nSP70-N (square), or nSP70-C (triangle) for 24 h was evaluated using the ^{3}H-thymidine incorporation assay. The percentage increase in cell proliferation was calculated relative to the negative control. Data are presented as means ± SD.
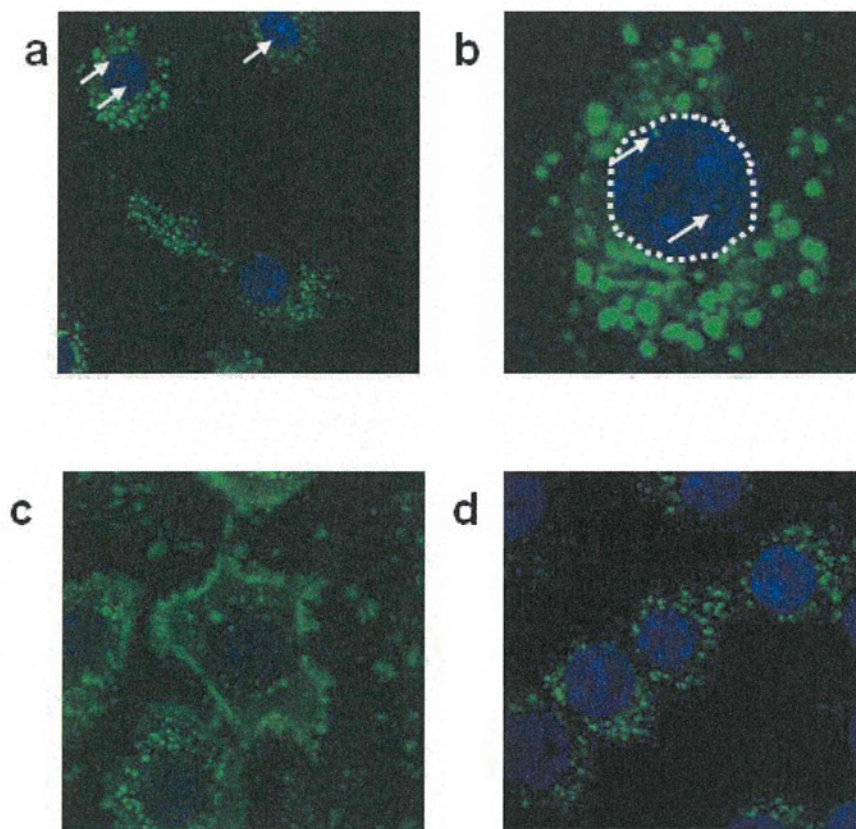
Figure 2 Localization of unmodified and modified nanosilica in RAW 264.7 cells. RAW 264.7 cells were treated for 3 h with 100 μg/ml of fluorescent (green-F)-labeled nSP70 **(a, b)**, nSP70-N **(c)**, and nSP70-C **(d)** (green). The nucleus was counterstained using DAPI (blue). The original magnification of these photographs was × 63 (a) and × 100 (c, d). (b) is a magnified image of a portion of photograph (a).

aggregation of intranuclear protein or inhibition of RNA transcription [26]. The said report [26] together with the results of this study suggests that silica nanoparticles enter the nucleus and induce inhibition of cell proliferation. Hence, the nSP70-mediated cytotoxic effect may be related to nuclear localization.

Investigating the cellular uptake/trafficking of individual nanosilicas is important for the development of safer forms of NMs. It is known that surface chemistry of nanoparticles, such as charge and the kind of modification group, affects their interaction with biological molecules [27]. For example, nanoparticles can induce different cellular responses by binding to proteins in the blood [28,29]. Bound proteins determine particle uptake by various cells and influence how nanoparticles interact with other blood components [30-32]. These findings suggest that surface modification alters the interaction between nanosilica and surrounding molecules, such as serum proteins, thereby altering the route of uptake into the cells. Mammalian cells ingest particulate matter by several routes, such as phagocytosis, macropinocytosis, clathrin-mediated, caveolin-mediated, and clathrin/caveolin independent endocytosis [33-35]. Each route involves a unique set of receptors and acts on particular types of particles. The authors anticipate that surface modification of silica nanoparticles will influence their interaction with bloodborne macromolecules. Thus, nanoparticles decorated with different macromolecules will have different intracellular distributions. The authors are currently investigating the effects of nSP70, nSP70-C, and nSP70-N on cytotoxicity, protein adsorption, cellular uptake, ROS generation, lysosomal stability, mitochondrial activity, activation of caspase 3 and 7, and mode of cell death (apoptosis versus necrosis).